

SYNTHESIS OF BISTRIPHENYLAMINE AND BENZODITHIOPHENE BASED
RANDOM CONJUGATED POLYMERS FOR
ORGANIC PHOTOVOLTAIC APPLICATIONS

A THESIS SUBMITTED TO
THE GRADUATE SCHOOL OF NATURAL AND APPLIED SCIENCES
OF
MIDDLE EAST TECHNICAL UNIVERSITY

BY

ASLI ÇETİN

IN PARTIAL FULFILLMENT OF THE REQUIREMENTS
FOR
THE DEGREE OF MASTER OF SCIENCE
IN
CHEMISTRY

AUGUST 2018

Approval of the thesis:

**SYNTHESIS OF BISTRIPHENYLAMINE AND BENZODITHIOPHENE
BASED RANDOM CONJUGATED POLYMERS
FOR ORGANIC PHOTOVOLTAIC APPLICATIONS**

submitted by **ASLI ÇETİN** in partial fulfillment of the requirements for the degree of
Master of Science in Chemistry Department, Middle East Technical University
by,

Prof. Dr. Halil Kalıpçılar
Dean, Graduate School of **Natural and Applied Sciences**

Prof. Dr. Cihangir Tanyeli
Head of Department, **Department of Chemistry**

Prof. Dr. Ali Çırpan
Supervisor, **Department of Chemistry, METU**

Examining Committee Members:

Prof. Dr. Levent Toppare
Chemistry Dept., METU

Prof. Dr. Ali Çırpan
Chemistry Dept., METU

Assoc. Prof. Dr. Yasemin Arslan Udum
Technical Science Vocation School, Gazi University

Assoc. Prof. Dr. Gülay Ertuş
Chemistry Dept., METU

Assoc. Prof. Dr. Görkem Günbaş
Chemistry Dept., METU

Date: 07/08/2018

I hereby declare that all information in this document has been obtained and presented in accordance with academic rules and ethical conduct. I also declare that, as required by these rules and conduct, I have fully cited and referenced all material and results that are not original to this work.

Name, Last name: Aslı Çetin

Signature:

ABSTRACT

SYNTHESIS OF BISTRIPHENYLAMINE AND BENZODITHIOPHENE BASED RANDOM CONJUGATED POLYMERS FOR ORGANIC PHOTOVOLTAIC APPLICATIONS

Çetin, Aslı

M. S., Department of Chemistry

Supervisor: Prof. Dr. Ali Çırpan

August 2018, 89 pages

Nowadays, traditional fossil fuels have become unable to compensate huge energy demand of the world due to the population increasing day by day and bringing about destructive greenhouse effect. Owing to all of these problems, renewable energy sources such as solar energy not only can be candidate for the solution of this expanded energy need but also can protect the earth by reducing the production of greenhouse gas. In this study, electronic, optical features and photovoltaic applications of two novel organic materials have been investigated to improve photovoltaic researches. With this aim, derivatives of bistriphenylamine, benzodithiophene as donor units and benzotriazole as an acceptor unit containing donor/acceptor (D/A) type random conjugated polymers, **P1** & **P2**, have been synthesized via Stille coupling reaction. The structure and the average molecular weight of these polymers have been examined with nuclear magnetic resonance spectroscopy (NMR) and gel permeation chromatography (GPC), respectively. Electrochemical characterizations of the polymers were investigated with cyclic voltammetry and also, UV-Vis-NIR spectrophotometer was used to determine optical features of the polymers. Electronic and optical band gaps of the polymers were recorded as 2.06 eV, 2.16 eV for **P1** and 2.16 eV, 2.11 eV for **P2**, respectively. In order to determine photovoltaic properties of

the polymers device fabrications were constructed with ITO coated glass substrate, PEDOT:PSS, (**P1** or **P2**):PC₇₁BM, LiF and Al in a given order. Photovoltaic performance of these polymer solar cell devices were measured under AM 1.5G solar irradiation of solar simulator via Keithler 2400 source meter. Photovoltaic studies showed that the highest power conversion efficiency (PCE) of these photovoltaic devices were recorded as 3.50 % with open circuit voltage; 0.79 V, short circuit current; 9.45 mA cm⁻², fill factor; 0.53 % for **P1**:PC₇₁BM (1:2, w/w) in 3 % *o*-dichlorobenzene (*o*-DCB) solution and 3.15 % with open circuit voltage; 0.75 V, short circuit current; 8.59 mA cm⁻², fill factor; 0.49 % for **P2**:PC₇₁BM (1:2, w/w) in 2% chlorobenzene (CB) solution.

Keywords: Benzotriazole, benzodithiophene, bistrisphenylamine, random conjugated polymer, organic solar cell, power conversion efficiency

ÖZ

BİSTRİFENİLAMİN VE BENZODİTİYOFEN BAZLI RASTGELE KONJÜGE POLİMERLERİN ORGANİK FOTOVOLTAİK UYGULAMALAR İÇİN SENTEZİ

Çetin, Aslı

Yüksek Lisans, Kimya Bölümü

Tez Yöneticisi: Prof. Dr. Ali Çırpan

Ağustos 2018, 89 sayfa

Günümüzde, geleneksel fosil yakıtlar gün be gün artan nüfus nedeniyle dünyanın büyüyen enerji ihtiyacını karşılayamaz olmuştur ve aynı zamanda yıkıcı sera gazı etkisini de beraberinde getirmiştir. Bu nedenle, güneş enerjisi gibi yenilenebilir enerji kaynakları artan enerji ihtiyacını karşılayabilecek bir seçenek olmakla beraber, dünyayı da sera gazı etkisinden koruyabilecektir. Bu çalışmada iki tane özgün organik malzemenin elektronik, fotovoltaik ve optik özellikleri araştırılmıştır. Bu amaçla, donör ünitesi olan bistrifenilamin ve benzoditiyofen ile akseptör benzotriazol türevlerini içeren donör/akseptör tipi serbest konjuge kopolimerler, **P1&P2**, Stille kenetleme reaksiyonu aracılığıyla sentezlenmiştir. Polimerlerin yapıları ve ortalama molekül ağırlıkları NMR spektroskopisi ve büyüklükçe ayırma kromatografisi ile incelenmiştir. Polimerlerin elektrokimyasal karakterleri dönüşümlü voltmetre kullanılarak belirlenmiştir. Ek olarak, polimerlerin optik özelliklerini belirlemek için UV-Vis-NIR spektrofotometresi kullanılmıştır. Elektronik ve optik bant aralıkları sırasıyla **P1** için 2.06 eV, 2.16 eV ve **P2** için 2.16 eV, 2.11 eV olarak kaydedilmiştir. Polimer güneş hücrelerinin fotovoltaik özellikleri Keithley 2400 fotometresi ile güneş simülasyonu olan AM 1.5 G aydınlatması altında gerçekleştirilmiştir. Fotovoltaik çalışmalar göre **P1:PC₇₁BM** (1:2) karışımı 0.79 V açık devre voltajı, 9.45 mA cm⁻² kısa devre akımı, 0.53 % dolun faktörü ile en yüksek güç dönüşüm verimi 3.50% iken

P2:PC₇₁BM (1:2) karışımı için 0.75 V açık devre voltajı, 8.59 mA cm⁻² kısa devre akımı, 0.49 % dolum faktörü ile bu verim 3.15% olarak kaydedilmiştir.

Anahtar kelimeler: Benzotriazol, benzoditiyofen, bistrifenilamin, rastgele konjüge polimer, organik güneş hücresi, güç dönüşüm verimi

To my precious family and Kağan...

ACKNOWLEDGMENTS

Foremost, I would like to state thankful to my advisor Prof. Dr. Ali Çırpan for his continues encouragement and invaluable guidance throughout my thesis study. I can never forget his valuable supports and advices that have given me in times where I am forced to decide about my future. It is a great honor to be his graduate student.

I am highly grateful to another respectable and valuable scientist Prof. Dr. Levent Toppare for his endless guidance and valuable advices about not only my thesis study but also my future plans.

I would like to thank Şevki Can Cevher and Emre Ataoğlu for their guidance, support and friendship during and after my thesis studies.

I am thankful to Dr. Şerife Özdemir Hacıoğlu and Çağla İstanbulluoğlu for their help and support in electrochemical and organic solar cell device studies.

I would especially like to thank amazing friends Özge Karagaçtı, Özge Azeri, Merve Bozdemir and Sinem Ulusan for being an important part of my happiest memories those will never forget through the rest of my life. I know that they will continue to be my best friends in every moment of my life.

Special thanks laboratory mates Soner, Kardelen, Ece, Janset, Sultan, Duygu, Merve, Duygu Güven, İpek and Dr. Fatma Demir for their friendships and an admirable working environment. I have always felt so special being a part of Cirpan Research Group.

There is one person I owe my special thanks to Kağan Gültekin for his excellent motivation, understanding, and invaluable love. Life is more beautiful and meaningful with his perfect friendship and true love.

I cannot explain my gratitude to my dear family with words. I always feel their invaluable love and support behind me. Being a part of such a endearious family is my

greatest chance in my life. Also, I would like to special thanks my nephew Asi for bringing me luck to my life.

TABLE OF CONTENT

ABSTRACT	v
ÖZ.....	vii
ACKNOWLEDGMENTS.....	x
TABLE OF CONTENT	xii
LIST OF TABLES	xv
LIST OF FIGURES.....	xvi
LIST OF ABBREVIATIONS	xix
CHAPTERS	
1. INTRODUCTION.....	1
1.1. Conjugated Polymers.....	1
1.2. Band Theory	2
1.3. Band Gap Engineering.....	3
1.4. Doping Process of Conjugated Polymers	5
1.5. Donor – Acceptor Approach.....	7
1.6. Moieties in Donor-Acceptor Approach Conjugated Polymers.....	9
1.6.1. Benzodithiophene Moiety	9
1.6.2. Triphenylamine Moiety.....	9
1.6.3. Benzotriazole Moiety	10
1.6.4. π Bridge Group: Thiophene.....	11
1.7. Derivatives of Triphenylamine, Benzodithiophene and Benzotriazole Containing Polymers	11
1.8. Electrochromism.....	20
1.8.1. Electrochromism of Conjugated Polymers	22
1.9. Important Parameters in Characterization of Electrochromic Materials	24
1.9.1. Electrochromic Contrast.....	24
1.9.2. Stability	24
1.9.3. Switching Time	25
1.9.4. Optical Memory	25

1.10.	Organic Solar Cells (OSCs)	25
1.10.1.	Operation Principle of OSCs.....	26
1.10.2.	Device Construction of Bulk Heterojunction OSCs	28
1.10.3.	Characterization of an Organic Solar Cell Device.....	29
1.10.4.	Important Parameters for OSC Efficiency	31
1.10.4.1.	Open-Circuit Voltage (V_{oc})	31
1.10.4.2.	Short-Circuit Current (J_{sc})	31
1.10.4.3.	Fill Factor (FF)	32
1.11.	Aim of the Study	32
2.	EXPERIMENTAL	35
2.1.	General	35
2.2.	Synthesis of Monomers	37
2.2.1.	Synthesis of 9-(Bromomethyl)nonadecane	37
2.2.2.	Synthesis of 4,7-Dibromobenzo[c][1,2,5]thiadiazole	38
2.2.3.	Synthesis of 3,6-Dibromobenzene-1,2-diamine.....	39
2.2.4.	Synthesis of 4,7-Dibromo-2H-benzo[d][1,2,3]triazole.....	40
2.2.5.	Synthesis of 4,7-Dibromo-2-(2-octyldodecyl)-2H- benzo[d][1,2,3]triazole.....	41
2.2.6.	Synthesis of Tributyl(thiophene-2-yl)stanne.....	42
2.2.7.	Synthesis of 2-(2-Octyldodecyl)-4,7-di(thiophen-2-yl)-2H- benzo[d][1,2,3]triazole.....	43
2.2.8.	Synthesis of 4,7-Bis(5-bromothiophen-2-yl)-2-(2-octyldodecyl)-2H- benzo[d][1,2,3]triazole.....	44
2.3.	Synthesis of Polymers	45
2.3.1.	Synthesis of P1	45
2.3.2.	Synthesis of P2	47
2.4.	Characterization of Conjugated Polymers.....	49
2.4.1.	Gel Permeation Chromatography.....	49
2.4.2.	Electrochemical Studies	49
2.4.3.	Spectroelectrochemical Studies.....	50
2.4.4.	Kinetic Studies.....	50
2.4.5.	Thermal Analysis	50

2.4.6. Photovoltaic Studies	51
3. RESULTS & DISCUSSION	53
3.1. Electrochemical Studies	53
3.2. Spectroelectrochemical Studies	55
3.3. Optical Studies	58
3.4. Kinetic Studies.....	59
3.5. Thermal Analyses of Polymers.....	62
3.6. Organic Solar Cell Device Applications	62
4. CONCLUSIONS	69
REFERENCES.....	71
APPENDICES.....	79
A. NMR DATA.....	79
B. THERMAL ANALYSIS RESULTS.....	88

LIST OF TABLES

TABLES

Table 1. Results of Electrochemical Studies of P1 and P2	55
Table 2. Results of Spectroelectrochemical Studies of P1 and P2	57
Table 3. Results of Kinetic Studies of P1 and P2	61
Table 4. Results of Photovoltaic Studies of P1	63
Table 5. Results of Photovoltaic Studies of P2	63

LIST OF FIGURES

FIGURES

Figure 1. Some of the Conjugated Polymers.....	2
Figure 2. Positive and Negative Polaron Formation	6
Figure 3. Electrochemical P and N-type Doping Mechanism (a) , Chemical P and N type Doping Mechanism (b)	7
Figure 4. Orbital Interactions in D-A Approach	8
Figure 5. Structure of Benzodithiophene Moiety	9
Figure 6. Structure of Triphenylamine Moiety	10
Figure 7. Structure of Benzotriazole Moiety	10
Figure 8. Molecular Structure of Thiophene Moiety	11
Figure 9. Structure of Poly(BTD-TPA)	12
Figure 10. Structure of P1	13
Figure 11. Structure of P2	13
Figure 12. Structure of P3	14
Figure 13. Structure of PV-BDTC1 and PV-BDTC2	15
Figure 14. Structure of T-PTB7 (31k)	16
Figure 15. Structure of P-BDTT₃-TPA	17
Figure 16. Structure of PBTD-BTz and PTIPSBTD-BTz	18
Figure 17. Structure of P4	19
Figure 18. Structure of PBTP1 and PBTP2	20
Figure 19. Electrochromic Behavior of WO ₃ and V ₂ O ₅	21
Figure 20. Redox Behavior of Viologens.....	22
Figure 21. Structure of PANI , PN-MePy and P3MeTh	23
Figure 22. Structure of PT and PEDOT	24
Figure 23. Working Principle of OSCs	27
Figure 24. Device Architecture of Bulk Heterojunction OSCs.....	29
Figure 25. Current Density-Voltage (J-V) Graph of OSCs.....	30
Figure 26. Illustration of AM 1.5 G	30
Figure 27. Structures of Synthesized P1 and P2	33
Figure 28. Synthetic Pathway of 9-(Bromomethyl)nonadecane	37
Figure 29. Synthetic Pathway of 4,7-Dibromobenzo[c][1,2,5]thiadiazole	38
Figure 30. Synthetic Pathway of 3,6-Dibromobenzene-1,2-diamine	39
Figure 31. Synthetic Pathway of 4,7-Dibromo-2H-benzo[d][1,2,3]triazole	40
Figure 32. Synthetic Pathway of 4,7-Dibromo-2-(2-octyldodecyl)-2H-benzo[d][1,2,3]triazole	41
Figure 33. Synthetic Pathway of Tributyl(thiophene-2-yl)stanne.....	42

Figure 34. Synthetic Pathway of 2-(2-Octyldodecyl)-4,7-di(thiophen-2-yl)-2H-benzo[d][1,2,3]triazole	43
Figure 35. Synthetic Pathway of 4,7-Bis(5-bromothiophen-2-yl)-2-(2-octyldodecyl)-2H-benzo[d][1,2,3]triazole.....	44
Figure 36. Synthetic Pathway of P1	45
Figure 37. Synthetic Pathway of P2	47
Figure 38. Single Scan Cyclic Voltammograms of P1 (a) and P2 (b) in 0.1 M TBAPF ₆ /ACN Electrolyte Solution at 100 mV s ⁻¹ Scan Rate.....	54
Figure 39. Electronic Absorption Spectra of P1 (a) and P2 (b) in 0.1 M TBAPFA ₆ /ACN Electrolyte Solution.....	56
Figure 40. The Colors of P1 (a) and P2 (b) upon Oxidation and Reduction with Their L, a and b Value	57
Figure 41. Normalized Absorption Spectra of P1 (a) and P2 (b) in Thin Film and CHCl ₃ Solution	59
Figure 42. Percent Transmittance Change (ΔT %) of P1 (a) and P2 (b) in 0.1 M TBAPF ₆ /ACN Electrolyte Solution at Maximum Neutral, Polaron, Bipolaron Absorption Wavelengths	61
Figure 43. TEM and AFM Images of P1 :PC ₇₁ BM (1:2 w/w) blend without treatment (a) with treatment (b). (Scale bars are 250 nm.)	65
Figure 44. TEM and AFM images of P2 :PC ₇₁ BM (1:2 w/w) blend without treatment (c) with treatment (d). (Scale bars are 250 nm.)	66
Figure 45. Current Density-Voltage (J-V) Behavior of P1 and P2 Based Best Performance Devices	67
Figure 46. ¹ H NMR of 9-(Bromomethyl)nonadecane	79
Figure 47. ¹³ C NMR of 9-(Bromomethyl)nonadecane.....	80
Figure 48. ¹ H NMR of 4,7-Dibromobenzo[c][1,2,5]thiadiazole.....	81
Figure 49. ¹³ C NMR of 4,7-Dibromobenzo[c][1,2,5]thiadiazole.....	81
Figure 50. ¹ H NMR of 3,6-Dibromobenzene-1,2-diamine.....	82
Figure 51. ¹³ C NMR of 3,6-Dibromobenzene-1,2-diamine.....	82
Figure 52. ¹ H NMR of 4,7-Dibromo-2-(2-octyldodecyl)-2H-benzo[d][1,2,3]triazole	83
Figure 53. ¹³ C NMR of 4,7-Dibromo-2-(2-octyldodecyl)-2H-benzo[d][1,2,3]triazole	83
Figure 54. ¹ H NMR of Tributyl(thiophene-2-yl)stanne.....	84
Figure 55. ¹ H NMR of 2-(2-Octyldodecyl)-4,7-di(thiophen-2-yl)-2H-benzo[d][1,2,3]triazole	84
Figure 56. ¹ H NMR of 4,7-Bis(5-bromothiophen-2-yl)-2-(2-octyldodecyl)-2H-benzo[d][1,2,3]triazole	85
Figure 57. ¹³ C NMR of 4,7-Bis(5-bromothiophen-2-yl)-2-(2-octyldodecyl)-2H-benzo[d][1,2,3]triazole.....	86
Figure 58. ¹ H NMR of P1	86

Figure 59. ^1H NMR of P2	87
Figure 60. TGA Curve of P1	88
Figure 61. DSC Thermogram of P1	88
Figure 62. TGA Curve of P2	89
Figure 63. DSC Thermogram of P2	89

LIST OF ABBREVIATIONS

CP	Conjugated polymer
BHJ	Bulk Heterojunction
OSC	Organic solar cell
EC	Electrochromic
OLED	Organic light emitting diode
OFET	Organic field effect transistor
PCE	Power conversion efficiency
D-A	Donor-Acceptor
HOMO	Highest occupied molecular orbital
LUMO	Lowest unoccupied molecular orbital
CB	Conduction band
VB	Valence band
WO ₃	Tungsten trioxide
BLA	Bond length alternation
CV	Cyclic voltammetry
ITO	Indium tin oxide
PSS	Polystyrene sulfonate
PEDOT	Polyethylene dioxythiophene
PCBM	[6,6]-Phenyl C 71 butyric acid methyl ester
TBAPF ₆	Tetrabutylammonium hexafluorophosphate

ACN	Acetonitrile
η_e	Power conversion efficiency
J_{sc}	Short circuit current density
V_{oc}	Open circuit voltage
FF	Fill factor
P_{max}	Maximum power
P_{in}	Power of the incident light
R_{sh}	Shunt resistor
R_s	Series resistor
AM 1.5 G	Air mass 1.5 global
E_g^{op}	Optical band gap
E_g^{el}	Electronic band gap
TGA	Thermal gravimetry analysis
DSC	Differential scanning calorimetry
UV	Ultraviolet
Vis	Visible
NIR	Near infrared
TPA	Triphenylamine
BDT	Benzodithiophene
BTz	Benzotriazole
BT	Benzothiadiazole
PPV	Poly(p-phenylene vinylene)
EQE	External quantum efficiency

CHAPTER 1

INTRODUCTION

1.1. Conjugated Polymers

Polymers are the products of chemical reactions taking place between simple, small repeating units named as monomers. Thanks to substantial properties of the macromolecules such as low weight, mechanical strength, resistivity, flexibility and low cost production they are widely used for industrial purposes.

Until discovery of conducting polymers, only those advantages of the conventional polymers could be utilized. This story started with a study conducted by Alan Heeger, Alan MacDiarmid, and Hideki Shirakawa and their discovery based on electrical conductivity of polyacetylene as a first conducting organic material via electrochemical doping process. After this outstanding discovery π -conjugated polymers opened new research area related with organic optoelectronic system for scientists. Superiority of conjugated polymers is based on electrical conductivity. Generally, conductivity of conjugated polymers can be explained with π -electron system which gives rise to formation of free charge carriers and electron delocalization ability. This conducting concept arises from presence of double and single covalent bonds between atoms on polymer main backbone, alternately. Overlapping between p_z orbitals of each sp^2 hybridized atoms in perpendicular position to the main backbone contributes π electron delocalization. Therefore, achievement of conduction property of conjugated polymers takes place by moving of these electrons through the polymer chain and also jumping from one chain to another.^{1,2} Furthermore, conjugated conducting polymers allow many optional synthetic ways in order to create them and extend conjugation length. Conjugated polymers used as an active part of optoelectronic system such as organic photovoltaic devices (OPV), organic light

emitting diode (OLED), organic field electronic transistor (OFET), electrochromic device (ECD) give many opportunities due to easy production, processability, simple modification ability, low priced and easy device fabrication.³ Some of the conjugated polymers are demonstrated in **Figure 1**.

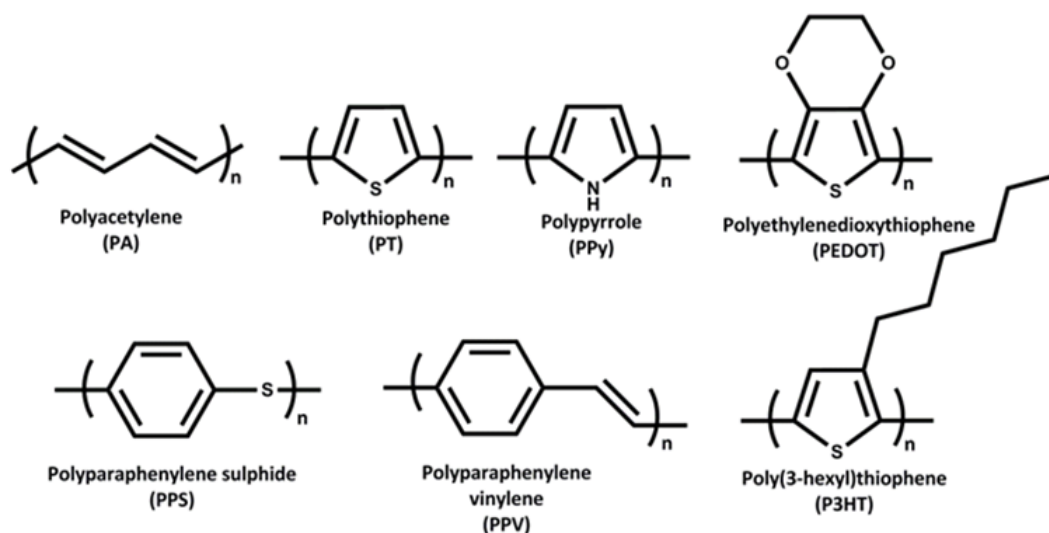


Figure 1. Some of the Conjugated Polymers

1.2. Band Theory

Solids demonstrate electrical conduction which can be explained via band theory as a function related to quantum theory (physical chemistry approach) or molecular orbital theory (chemical approach). Quantum and molecular orbital theory clarify the conduction property of a solid through atomic orbital energy levels and molecular orbitals arising from combination of atomic orbitals, respectively. Generally, both of the theories explain that conductivity is associated with energy differences between valence and conduction bands. To put it another way, band gap is equal to difference between valence band (VB) as bonding orbital and conduction band (CB) as

antibonding orbital named highest occupied molecular orbital (HOMO) and lowest unoccupied molecular orbital (LUMO), respectively.⁴

Classification of the materials as insulator, conductor, and semiconductor is performed with this theory. In insulator type materials, there is no electrons occupied in CB while electrons fill VB completely. Normally, thermal or photochemical applications can bring about electron jumping from VB to CB by exciting electrons if energy separation between these bands is acceptable. However, even if any process is applied insulators to excite its electron, promotion of electrons to CB cannot achieve owing to larger band gap energy ($E_g > 3.0$ eV). Therefore, they do not possess electrical conduction feature. Unlike insulator, metals known as conductor materials have partially filled overlapping band and therefore, electrons can reach all of the energy levels. Owing to band overlapping there is no energy separation between the bands ($E_g = 0.0$ eV). Partially filled VB, empty CB and small band gap (E_g) being in the range of 1.0-3.0 eV are characteristic feature of semiconductors. Conducting polymers having extended conjugation are in the semiconductor group and can conduct electricity by creating charge carriers. When one of the excitation methods is applied to polymers, electrons promote to CB and holes remains in the VB. Therefore, electrons can travel through the polymer chain, which cause conductivity. Doping process discussed in following section is another way to form holes and electrons.⁵

1.3. Band Gap Engineering

HOMO/LUMO energy levels and band gap of conjugated polymers determine their photovoltaic performances since optical and electronic features being curtail parameters for optoelectronic systems is based on position of these energy levels and space between them. Main concern of the band gap engineering is related with creating conjugated polymers with low band gap by alternating the positions of HOMO/LUMO energy levels. When band gap concept can be concern, bond length alternation (E_{BLA}), resonance energy (E_{Res}), planarity and dihedral angle (E_θ), intermolecular interaction (E_{Int}) and substitution effect (E_{Sub}) as structural properties become important

parameters since strategies to low band gap is developed by controlling these factors. Planarity, dihedral angle, quinoid form's controlling, incorporation of electron deficient and rich moiety are the key strategies.⁶ Contribution of the each factors to band gap energy is represented as **Eq 1**⁷.

$$\mathbf{E_g = E_{BLA} + E_{Res} + E_{\theta} + E_{Int} + E_{Sub} \quad \mathbf{Eq. 1}}$$

Actually, band gap energy of the conducting materials such as polyaromatic conjugated polymers results from synchronic double and single bonds between C atoms of the main chain. Unlike the non-polyaromatic materials, these polyaromatic conjugated systems illustrate two main resonance form namely aromatic and quinoid at their non-degenerate ground states. These two structures show non-identical effect on band gap due to their different resonance energy. If comparison of the aromatic and quinoid forms is performed regarding stabilization in energy, former is energetically more stable and hence its contribution to the band gap energy is higher. However, quinoid form of mesomeric structure leads to lower in band gap energy because of absence of stabilization energy. Resonance stabilization energy adjusts the alternation of aromatic and quinoid form. That is, tendency of limiting the electron in aromatic structures of polyaromatic conjugated polymers increases with high resonance energy and hence, energy separation between HOMO and LUMO levels become higher with leaning of aromatic form.⁷

Bond length alternation (BLA) as an effective geometric parameter for the band gap energy is expressed in terms of differences between average bond length of neighboring carbon-carbon atoms. In other words, representation of aromatic to quinoid population ratio of the polyaromatic conjugated systems is given with BLA factor. When the quinoid form is predominant in the polyaromatic system, double bond tendency between two neighboring aromatic ring is higher. Therefore, band gap energy starts to decrease with decreasing BLA value. Indeed, resonance stabilization energy and BLA cannot be considered apart from each other since decreasing in the aromatic stabilization energy causes less aromaticity on main chain and lower BLA value due to higher quinoid population. Addition of non-aromatic conjugated part to aromatic system is a strategy to reduce aromaticity and enhance quinoid form.⁸

With a purpose of extending the conjugation and assisting electron delocalization through the main chain, parallel π -orbital interactions taking place between neighboring aromatic systems can be developed with increasing planarity of the chain. Hence, low BLA and reduced band gap energy are occurred with reduced planarity. Furthermore, these poly aromatic systems are exposed to rotational disorder on a single bond between two adjacent aromatic units. This resultant dihedral angle gives rise to restriction of electron delocalization through the polymer chain and increases band gap energy. In order to overcome this problem an important strategy named chemical rigidification is applied by forming covalent bond between two aromatic units. Thanks to the strategy low energy gap between frontier levels is obtained.^{7,9}

Substitution effect is another parameter to control the band gap. Frontier orbital of the conjugated polymers can be modified with variation of substitution on aromatic units of conjugated system. While electron withdrawing groups on aromatic rings cause large increment in oxidation potential of aromatic moiety, decreasing in this potential is observed due to electron releasing group. Thereby, position of HOMO level can be raised with electron rich substituents but electron deficient substituents can cause low lying LUMO level so that band energy decreases.¹⁰

Solid or solution form of the conjugated polymers affects their ordered structures and band gap energies. Increasing in the chain interaction becomes possible when the polymer chains are in solid form since all the chains are closer to each other in a solid form compared to those in a solution. Rise in the inter-chain electron delocalization causing low energy between frontier orbitals results from enhancement of intermolecular interaction of conjugated polymers being in solid form.¹¹

1.4. Doping Process of Conjugated Polymers

The most important distinguishing feature between conjugated polymers and other types of polymers is electrical conduction ability of the conjugated materials. However, at ground or undoped state of the conjugated materials their π -electrons are

not delocalized along the main backbone of the polymer chains therefore they behave as an insulator. In spite of their electrical insulation at their ground state, conducting feature can be gained to them with doping strategy by creating free charge carriers namely single charged polarons and double charged bipolarons. Thanks to this strategy, conductivity region of the polymers can be increased from insulator region to metallic region.¹³ Positive and negative polaron formation is shown in following **Figure 2**.

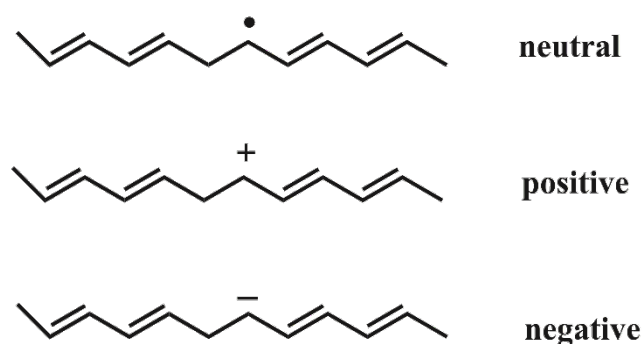


Figure 2. Positive and Negative Polaron Formation

The mobile charge forming process can be implemented by oxidation/reduction reactions via electrochemical or chemical methods. When electrons are removed from the HOMO energy level of conjugated polymers, this process is known as p-type doping. If electrons are injected to LUMO energy level of conjugated materials name of the process become n-type doping. During p and n-type process holes and electrons are generated as free charges, respectively and neutralization of them is performed with counter charges named dopant.¹⁴

Electrochemical p and n-type doping are performed by applying positive and negative voltage, respectively and transportation of counter ion dopant through the electrolyte solution become important to achieve this process. Unlike the electrochemical type doping, doping via chemical method is succeeded by utilizing oxidative (Br_2 , I_2) dopants for p doping and reductive (Na, Li) dopants for n doping. In this case, introduction of chemical dopant into conjugated materials is performed by subjecting

to vapor or solution of the dopants.¹⁵ Detailed demonstration of electrochemical and chemical doping mechanism is in **Figure 3**.

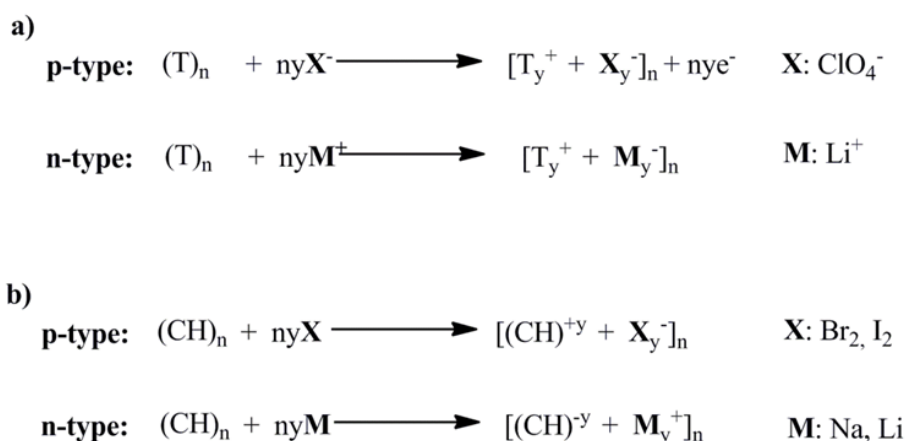


Figure 3. Electrochemical P and N-type Doping Mechanism (a), Chemical P and N type Doping Mechanism (b)

1.5. Donor – Acceptor Approach

In order to improve device performances of polymer based solar cells (PSCs), designing of conjugated polymers is a key parameter to create semiconductors having suitable band gap, wide light harvesting and advance charge transporting ability. With this aim, conjugated polymers used as electron donating moiety in solar cell are designed with some structural modification by utilizing different methods. Donor-Acceptor (D-A) approach as one of the most efficient method is frequently applied to augment the PCE by lowering the band gap of the synthesized polymers and improving light absorptivity.¹⁶ Thanks to this strategy, controlling of electron delocalization, bond length alternation and quinoid structure can be achieved by introducing electron deficient A and electron rich D moieties on the some polymer backbone alternatingly or randomly. Suitable matching between D units with high HOMO energy level and A units with low LUMO level is keystone to obtain lower band gap. Lower band gap

conjugated polymers resulting from this approach can be attributed hybridization of HOMO-LUMO energy levels. The reason of the hybridization forming new energy levels is related with strong interaction between electron rich D and deficient A sequences.¹⁴ Hybridization of energy levels of D-A units and new forming HOMO-LUMO energy levels are illustrated in **Figure 4**.

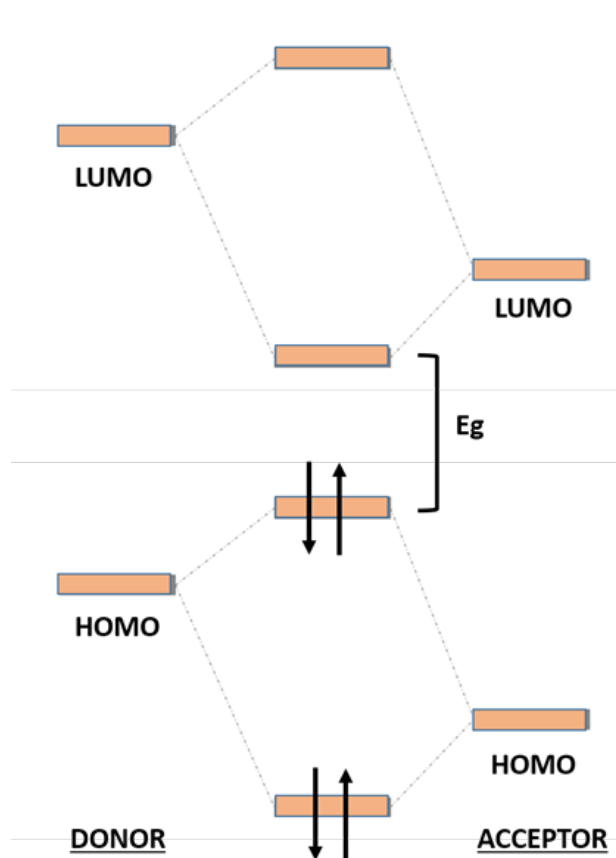


Figure 4. Orbital Interactions in D-A Approach

In this approach, many examples which has promising electron rich D moiety having high V_{oc} such as benzodithiophene (BDT), carbazole, fullerene and heteroaromatic electron deficient A moiety like benzotriazole, diketopyrrolopyrrole, quinoxaline, 2,1,3 benzothiadiazole, triphenylamine derivatives etc. present alternatingly on the main backbone of the polymer chain.^{17,18}

1.6. Moieties in Donor-Acceptor Approach Conjugated Polymers

1.6.1. Benzodithiophene Moiety

Π -conjugated benzodithiophene (BDT) containing polymers demonstrate advanced photovoltaic performance since BDT derivatives have high hole mobility due to their extraordinary planar nature. Additionally, simple conjugated side groups' incorporation with BDT unit can enhance planarity of the polymer and adjust energy levels of frontier orbital. Thanks to having wide planar structural morphology of BDT, π - π stacking gets easier. Except from that property, attachment of alkoxy unit at 4 and 9 position of the benzene in BDT moiety can downscale the band gap by minimizing the effect of steric hindrance and enhance the solution processability of the polymers.^{19,20} Structure of BDT moiety is illustrated in **Figure 5**.

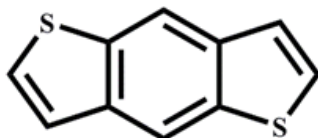


Figure 5. Structure of Benzodithiophene Moiety

1.6.2. Triphenylamine Moiety

In the literature, triphenylamine (TPA) and its derivatives are extensively utilized for organic light emitting diodes (OLEDs)²¹, organic solar cells²², organic field effect transistor²³ and electrochromic applications²⁴ since TPA containing materials demonstrate unlabored oxidation capability through the nitrogen center and extremely immense hole mobility.²⁵⁻²⁷ In addition to this, TPA derivatives indicate considerable high LUMO energy level, which brings about well electron blocking character. Moreover, conjugated polymers with triphenylamine moiety are possessed of splendid electrochemical and thermal stability.²⁸ Structure of TPA unit is shown in **Figure 6**.

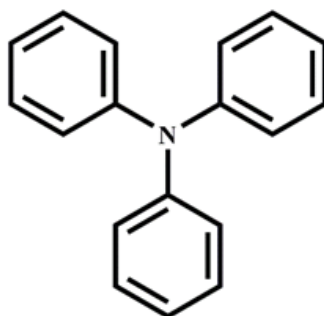


Figure 6. Structure of Triphenylamine Moiety

1.6.3. Benzotriazole Moiety

Benzotriazole (BTz) moiety incorporated with different molecules is very useful material for photoelectronic applications.^{29,30} According to recent studies electron deficient heteroaromatic benzotriazole (BTz) and its derivatives are frequently utilized in the organic optoelectronic systems by the reason of powerful electron accepting and transporting nature of BTz. Benzothiazole (BT) containing polymers having higher electron accepting strength have been demonstrated better PCE than polymers with BTz unit; however, due to capability of functionalizing N-H bond on the triazole ring of BTz unit, electronic nature and solubility of the polymers can be easily improved.^{31,32} Structure of BTz moiety is shown in **Figure 7**.

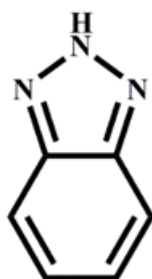


Figure 7. Structure of Benzotriazole Moiety

1.6.4. π Bridge Group: Thiophene

Polymers involving heterocyclic conjugated units such as thiophene, thieno[3,2-*b*]thiophene, furan, selenophenes³³ etc. have been shown better electronic and optical property because of π bridge's effect. These conjugated linkers can advance the interaction between D and A units, thereby improving charge transport, electrochemical and photovoltaic character of the polymers. Furthermore, planarity of polymer chain can be increased with these heterocyclic moieties. Therefore, owing to the easier overlapping between π orbitals of neighboring atoms HOMO energy level is at low lying position and red shifted absorption are observed compared to the polymers without π bridges.³⁴ Molecular structure of thiophene is illustrated in **Figure 8**.



Figure 8. Molecular Structure of Thiophene Moiety

1.7. Derivatives of Triphenylamine, Benzodithiophene and Benzotriazole Containing Polymers

Star or branched shaped triphenylamine (TPA) derivatives are widely used as donor building block for polymer or small molecule based optoelectronic systems. Sterically hindered phenyl units of TPA moiety gain nonplanar propeller shaped to molecule incorporated with TPA derivatives. Besides, this unit illustrates strong hole transporting ability owing to easy oxidized nitrogen atom and transportation capability of holes via stable cations. Additionally, photovoltaic performances of materials containing this unit can be studied without preannealing.³⁵ Yasuda and coworkers have

shown independency of TPA containing polymers ((**Poly(BTD-TPA)**)) shown in **Figure 9** from solvent type and annealing temperature. Device fabrications and annealing of **Poly(BTD-TPA):PC₇₀BM** (1:4, w/w) were done with CHCl₃ and o-DCB at 60 °C and 110 °C for 10 min, respectively. PCE of these two devices were almost same and recorded as 2.81 % for device with CHCl₃, 2.65 % for device with o-DCB.³⁶

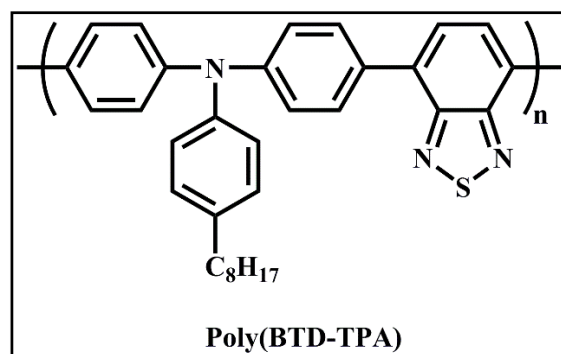


Figure 9. Structure of **Poly(BTD-TPA)**

Furthermore, Zang et al. designed TPA and benzothiadiazole containing polymer (**P1**) illustrated in **Figure 10** and investigated the photovoltaic performance of the material. They obtained the highest PCE as 3.37 % with quite high V_{oc} ; 0.90 V.³⁷ Wang and coworkers' studies examined the effect of phenyl moiety around the nitrogen atom in phenylamine molecule. According to the results triphenylamine moiety showed higher V_{oc} and PCE compared to diphenylamine unit since formation of larger free space among the polymer chains allowed fullerene molecule to distribute within these free space, effectively.²² Structure of synthesized polymers shown in **Figure 11** and **Figure 12**.

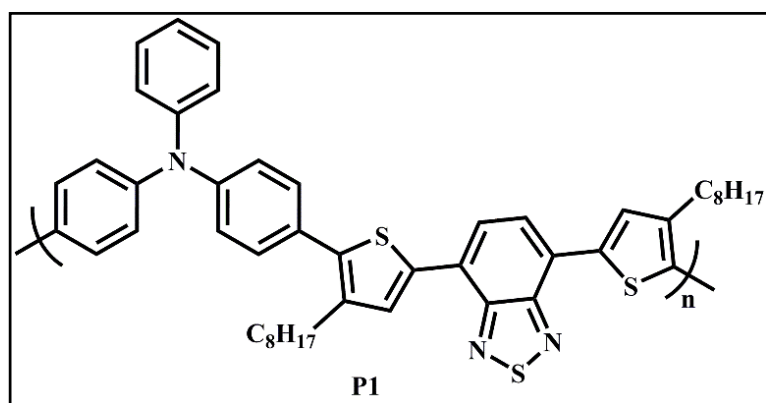


Figure 10. Structure of **P1**

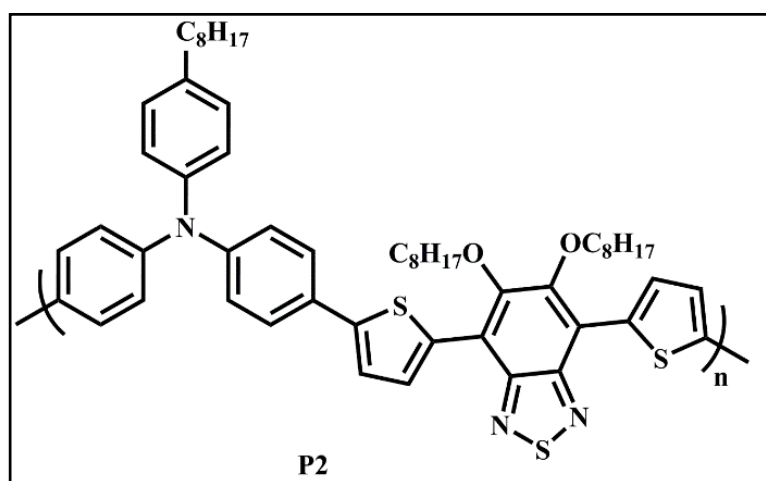


Figure 11. Structure of **P2**

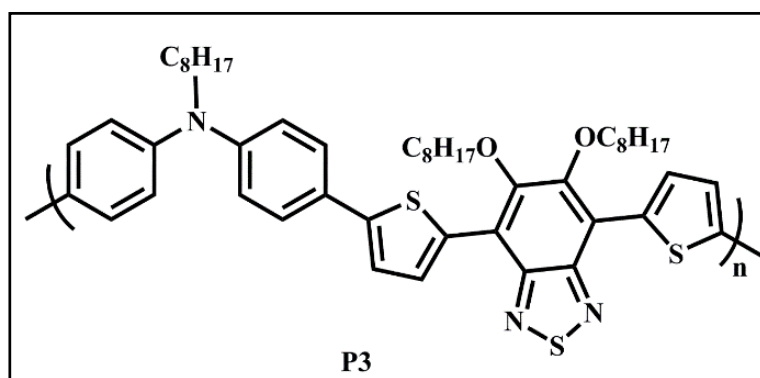


Figure 12. Structure of **P3**

Benzodithiophene (BDT) moiety can be shown as the most powerful promising donor units for organic materials such as conjugated polymers or small molecules since BDT has symmetrical planar structure and prolonging conjugation length. Furthermore, organic materials involving BDT unit exhibit high PCE with low lying HOMO level and high V_{oc} .³⁸ Toa et al. synthesized BDT incorporated D-A type conjugated polymers shown in **Figure 13** with high V_{oc} range between 0.93 V-1.04 V and relative low HOMO energy levels.³⁹ Another study performed by Raj and coworkers revealed BDT containing polymer pointed 7.8 % PCE with great J_{sc} (15.2 mA cm⁻²) (**Figure 14**).⁴⁰

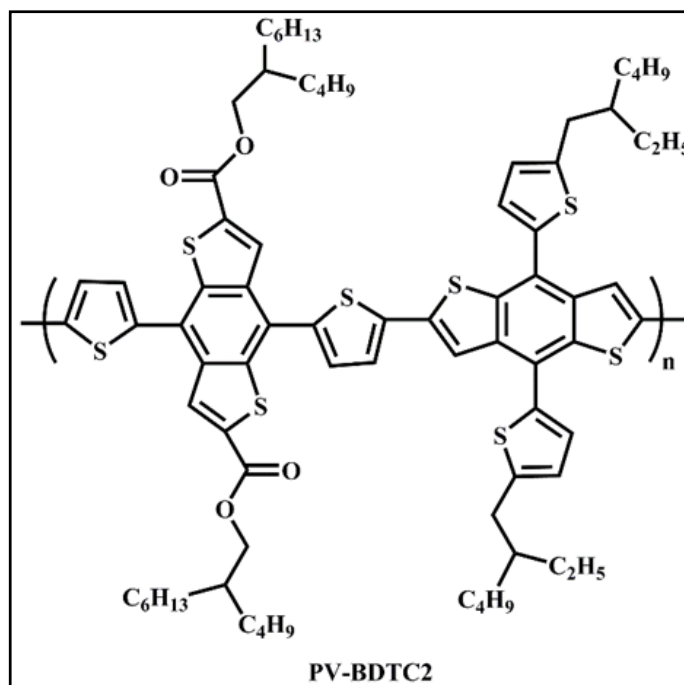
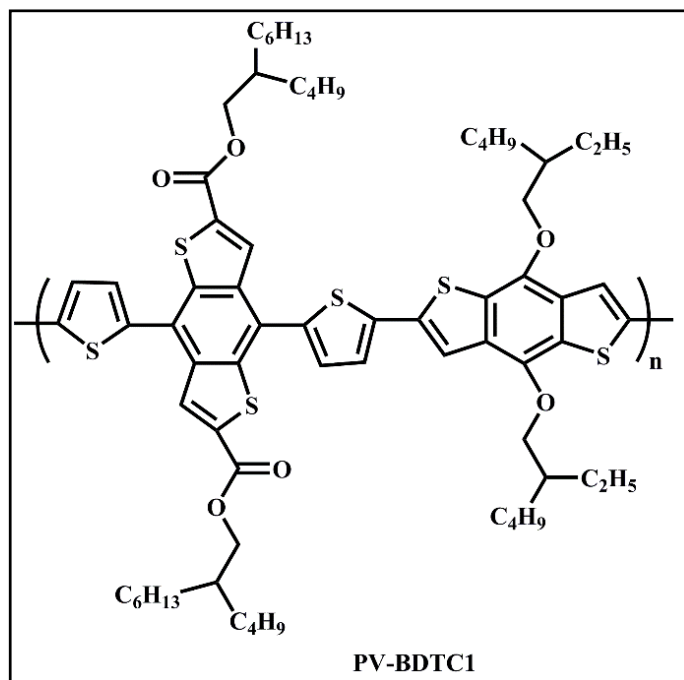


Figure 13. Structure of **PV-BDTC1** and **PV-BDTC2**

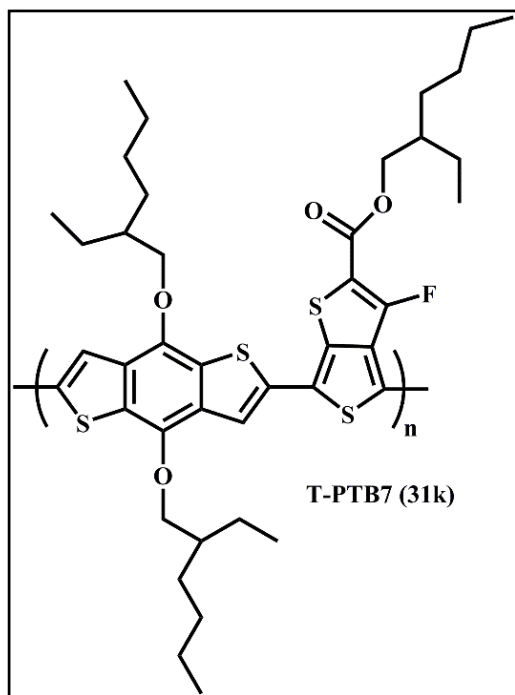


Figure 14. Structure of **T-PTB7 (31k)**

Wang and coworkers were conducting a study in which the attachment of conjugated side chains such as thiophene, benzothiadiazole etc. on the molecules rather than 4 and 9 positions of BDT unit widen the absorption region and reduce the HOMO/LUMO energy levels of BDT containing polymers. However, this strategy reduced planarity of the polymer owing to steric hindrance effect of introduced conjugated side chains with alky side chains on BDT unit. Hence, this polymer exhibited quite high V_{oc} and J_{sc} but limited FF. In order to solve the FF problem planarity of the polymer main backbone increased with triphenylamine derivative. According to the results, extended $\pi \pi^*$ transitions, high hole mobility ($1.06 \times 10^{-2} \text{cm}^2 \text{V}^{-1} \text{s}^{-1}$) with ordered structure and considerable high FF were recorded.⁴¹ Synthesized polymer **P-BDTT₃-TPA** was shown in **Figure 15**.

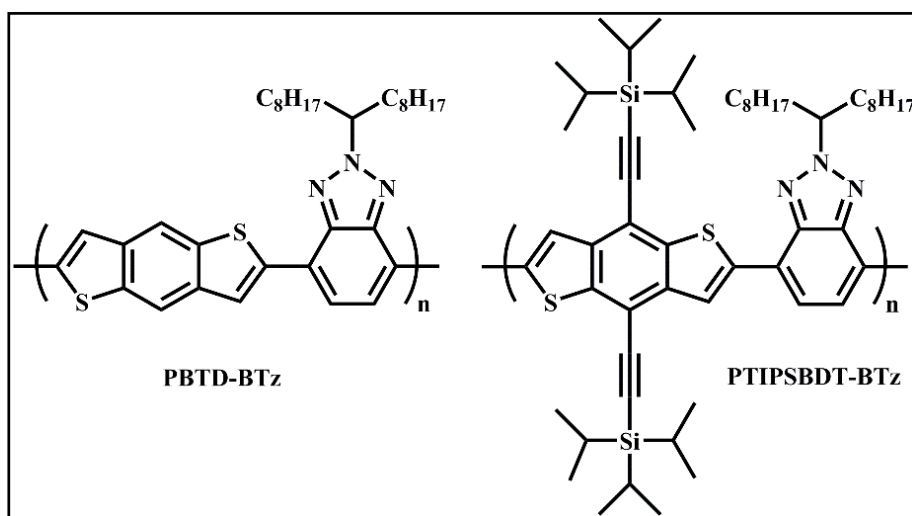


Figure 16. Structure of **PBTD-BTz** and **PTIPSBTD-BTz**

Kotowski and coworkers reported synthesis of BTz, benzothiadiazole and BDT containing random terpolymer with effective photovoltaic results. Combination of BTz and benzothiazole units as acceptors led to enhancement of interactions between D and A sides on the polymer backbone and improvement of polymer fullerene mixing morphology. Due to the presence of BDT unit π conjugation improved and suitable band gap obtained. Performance of bulk heterojunction solar cell constructed from polymer demonstrated in **Figure 17** was recorded as 5% PCE with admirable J_{sc} (10.30 mA cm⁻²) and high V_{oc} (0.80 V).⁴⁴

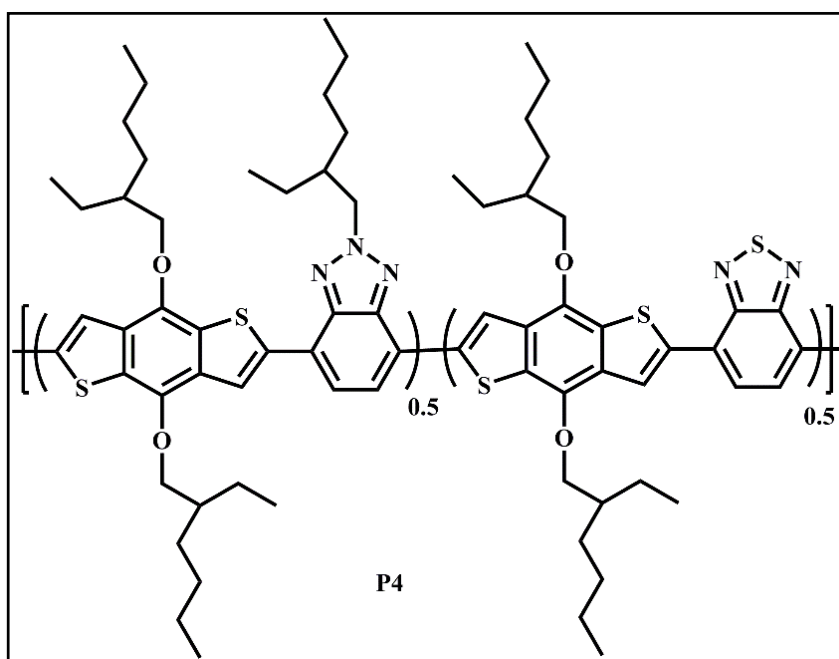


Figure 17. Structure of **P4**

Presence of π -bridges between A and D moiety is a common strategy to adjust the HOMO/LUMO energy levels, band gap and expand light absorption ability of the organic materials. An article published in 2017 by Goker et al. concluded that effect of π -bridge on electronic and optical properties of the polymers. When conjugation length increased with π -bridge, photovoltaic performance of the polymers was improved, linearly. PCE % of single and two thiophene containing TPA and BTz based polymers were recorded as 2.27 % and 3.65 %, respectively. Furthermore, when comparison of these two polymers was carried out, huge development on J_{sc} with increasing conjugation length and smaller optical band gap was easily observed. J_{sc} of one and two thiophene incorporated polymers were recorded as 8.19 mA cm⁻² and 14.73 mA cm⁻², respectively.⁴⁵ Structure of these π -bridge attachment polymers were shown in **Figure 18**.

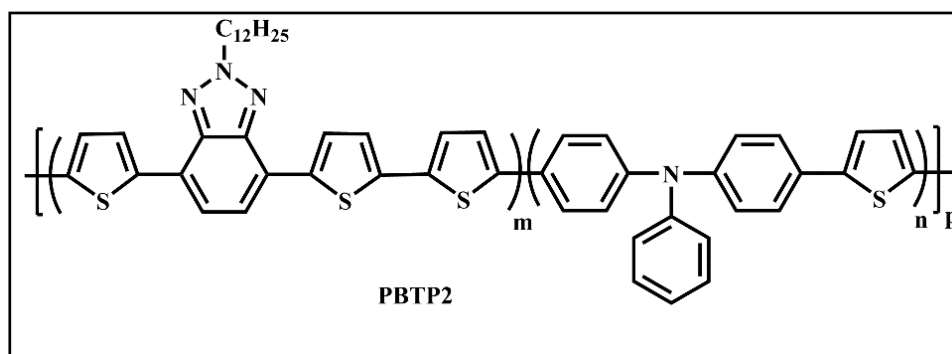
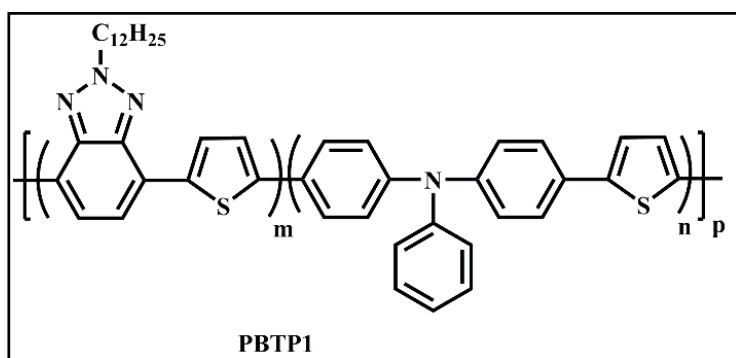


Figure 18. Structure of **PBTP1** and **PBTP2**

1.8. Electrochromism

Electrochromism is defined as reversible, persistent and visible change in optical behaviour of electrochromic materials when they are exposed to electrochemical oxidation and reduction process. During the redox switching different electronic absorption bands in visible region give rise to color change between two colored states or mainly a colored and transparent state. Sometimes such materials can have not only one redox state but also multiple redox states which are named as poly electrochromic or multi electrochromic materials. Therefore, these materials possess more than one color on switching between multiple redox states.⁴⁶

Electrochromic materials attract the attention of industry and science world due to their remarkable spectroelectrochemical features and they are frequently used in smart windows, electronic display, electronic paper and optical shutter technology.

Transition metal oxide films, viologens and conjugated polymers can be shown as three main classes of the electrochromic materials.⁴⁷

Deb and coworkers studies demonstrated that amorphous and crystalline metal oxides were the first candidates for electrochromic device. Transition metal oxides especially tungsten trioxide (WO₃) with high band gap demonstrates transparent feature in visible region.⁴⁸ However, colour switching of WO₃ from transparent to intense blue can be observed when W⁺⁶ is electrochemically reduced to generate W⁺⁵. Additionally, vanadium pentoxide (V₂O₅) can show cathodically colouring behaviour. Unlike WO₃, colour switching of V₂O₅ occurs between two coloured states. Brown and blench blue are the oxidized and reduced colour of V₂O₅, respectively. Similar to W and V, oxide of Mo, Nb, and Ti can generate colour upon electrochemically reduction and they are named as cathodically colouring transition metal oxides. However, oxide of Ni, Co, Ir can be categorized as anodically colouring transition metals.⁴⁹ Electrochromic behaviors of WO₃ and V₂O₅ were illustrated in **Figure 19**.

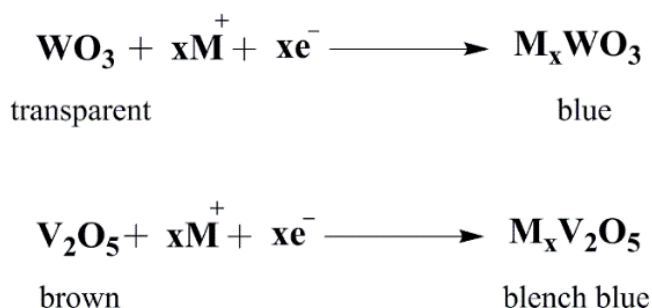


Figure 19. Electrochromic Behavior of WO₃ and V₂O₅

The doping viologens (bipyridiliums) demonstrate electrochromic redox activity due to their special structures. After redox activity of these molecules were discovered in 1933 detailed investigations on them were performed over the years. This electrochromic feature of the viologens is a result of formation of radicalic cations via electrochemical reduction process. Simplest chemical structure and radicalic cation

formation from the most stable dication of viologens is shown in **Figure 20**.^{50,51} Color variety of thin film viologens results from the different type substitute the N position of viologens. To illustrate, attachment of n-heptyl on viologen possess purple color at its radical cation form whereas its dication and neutral form show transparency.⁵²

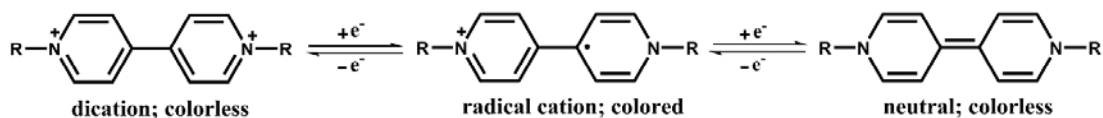


Figure 20. Redox Behavior of Viologens

1.8.1. Electrochromism of Conjugated Polymers

Conjugated polymers have become very popular among the electrochromic devices owing to their high optical contrast, quick response time and more processable opportunity. Rather than these advantages of CPs, their multichromic features resulting from the structural modification ability and long life time property can be distinguished from the other electrochromic materials. For example, thin film of polyaniline (**PANI**) (**Figure 21**) shows multiple colors depending upon its oxidation states, which involves bright yellow, green, and dark blue color. Moreover, poly(N-methylpyrrole) (**PN-MePy**) and poly(3-methyl-thiophene) (**P3MeTh**) (**Figure 21**) possess extremely high stability and reversible electrochromism. Electrochromic switching of the conducting polymers arises from creation of polaron and bipolaron via redox processes since these new charge carriers bring about optical and optoelectronic modifications.^{53,54}

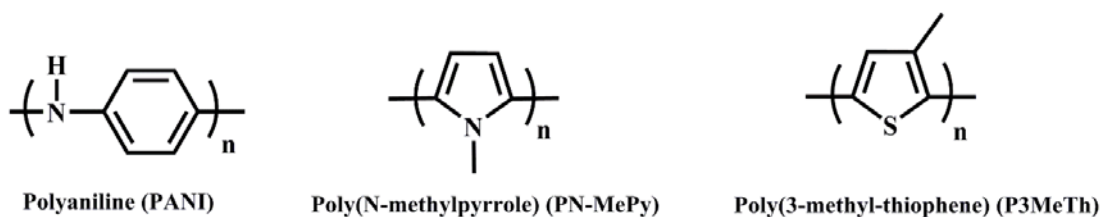


Figure 21. Structure of **PANI**, **PN-MePy** and **P3MeTh**

Color controlling of electrochromic CPs can be achieved by applying three major strategies. Firstly, colors of the polymers are directly related with the band gap and therefore, tuning of the band gap via structural modifications is mainly applied strategy. Steric and electronic effects of substituents designate the electron density on the polymer chains and effective conjugation length. Hence, band gap between HOMO and LUMO energy levels and optical absorption region can alter. To illustrate, polythiophene (**PT**) with 2.0-2.2 eV band gap shows red, blue and green color in the neutral, oxidized and reduced states, respectively. If **PT** is incorporated with electron donating ethylenedioxy units band gap of new cathodically coloring CP (poly(3,4-ethylene-dioxythiophene) (**PEDOT**)) is obtained as 1.6 eV. When **PEDOT** is oxidized from neutral state, its color turns from blue to transparent (**Figure 22**).⁴⁸ Secondly, copolymerization is another method for controlling the electrochromic properties of CPs since combination of different properties of the monomers leads to variety in optoelectronic features. Additionally, color controlling of the CPs which consist of thiophene, carbazole and pyrrole derivatives can be obtained by modulating the monomer ratio. Thirdly and finally, blends and composites of the polymers having different color regions can combine the electrochromic properties of these systems. This simplest strategy is mainly preferable to create multicolor electrochromic CPs.⁴⁶

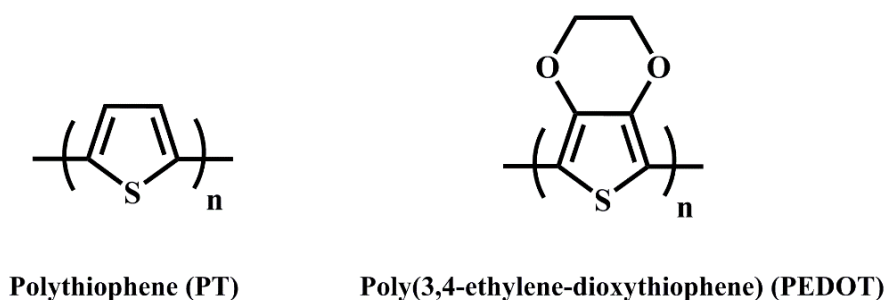


Figure 22. Structure of **PT** and **PEDOT**

1.9. Important Parameters in Characterization of Electrochromic Materials

1.9.1. Electrochromic Contrast

Electrochromic or optical contrast is preferential factor among processes used to evaluate electrochrome. Reporting of this parameter is commonly given as percent transmittance change ($\Delta T\%$) at a specified wavelength where the highest optical contrast of the material is recorded. Measuring the change in the relative luminance offers an opportunity related with obtaining of overall optical contrast of the electrochrome. Percent transmittance is generally obtained as cycles when square wave potentials are applied to electroactive materials within spectrophotometer. These cycles can be monitored at different wavelengths and varied potentials. Percent transmittance give an additional information about the optical stability of the materials.⁵⁵

1.9.2. Stability

Electrochromic and electrochemical stability of the electroactive materials are the key factors for the device performances since reduction of the optical contrast and poor device performance is due to the degradation of redox couple of the active layer. Irreversible redox feature at extremely high potentials, deterioration of the electrode or evaporation of electrolyte solution, side reactions due to the availability of

oxygen/water in the cell and production of heat on the resistive parts can be denotable as the reasons of degradation. Therefore, air and water free capsuling of the electrochromic devices, flawless processing and attentive charge balance of the active layer are the crucial parameters for the long-term electrochromic device performances.⁴⁸

1.9.3. Switching Time

Switching time or speed which has a great significance for display applications, electrochromic shutters and switchable mirrors is defined as a time needed for observing the colors switching of the electrochrome via oxidation and reduction processes. Ionic conductivity of electrolyte, ion diffusion toward the active sides along the thin film, active layer thickness and surface morphology are the parameters affecting the switching time.¹¹

1.9.4. Optical Memory

Definition of optical memory (open-circuit memory) of the electrochrome is explained as tendency of a material to maintain its colored or bleached state without external electric field. Colored state of solution based electrochromic devices bleaches quickly compared to the solid state based devices due to free electrochrome diffusion ability and high self-erasing mechanism (electron exchanging) of the solution based devices.⁴⁸

1.10. Organic Solar Cells (OSCs)

Solar energy as one of the renewable energy sources has been very popular subject owing to rapidly growing energy needs of the world population and accelerating environmental problems arising from combustion of fossil fuels. In order to overcome this global energy problem with an environmental way, solar cell technology has been seen as a remarkable and promising solution. Power conversion efficiency (PCE) of the inorganic solar cell as a comparatively mature photovoltaic technology has been

recorded just above 25% for silicon based inorganic solar cell and 42.3% for heterojunction type inorganic solar cell. Although inorganic based technology achieves high PCE it has significant problems like inconvenient fabrication process, expensive manufacturing, rigidity and disability of large size fabrication.⁵⁷ Organic solar cell, especially polymer containing one, is ahead of the other solar cell technology due to its cost effectiveness, easy manufacturing, solution processability, light weight, ability of large area fabrication and flexible design.⁵⁸ Development of device architecture of the organic solar cell is single layer, bilayer and bulk heterojunction, chronologically. Except from the single layer type organic solar cell, the other types have donor and acceptor in the active matrix. The bilayer architecture possesses some problems related with exciton diffusion length and thickness of active matrix and therefore, these problems lead to low PCE. In order to achieve the problems of bilayer architecture bulk heterojunction type organic solar cell has been discovered by Yue and coworkers in 1995. In this type architecture, active matrix is formed from donor and acceptor materials which are in a blended form.^{59,60}

1.10.1. Operation Principle of OSCs

Operation principle of an organic solar cell involves four major steps, basically. This operation starts with light absorption of the active layer and continues with the generation of excitons which are electrostatically coupled electron hole pairs. In this step, optical band gap of the donor moiety must match the incident photon energy of the light in order to excite electron of the donor part in the active layer. After electron of the donor moiety is excited by the photon energy from the highest occupied molecular orbital (HOMO) to the lowest unoccupied molecular orbital (LUMO), the excited electron and the remaining hole are bounded, coulombically. These creating excitons need to be energized more than 0.5-1.0 eV to form free electrons and holes.

Second step of the operation is the exciton diffusion toward donor-acceptor (D-A) interface in the active layer to form free charges. Diffusion length of these photogenerated excitons is 5-20 nm. If excitons travel more than 20 nm they may be

recombine or loss their energy as heat. Therefore, morphology of the active layer is an important parameter for high efficiency solar cell.

Third step is related with the exciton dissociation to form free charges at the interface of the D-A moieties. LUMO levels of the D-A moieties should be different from each other and higher than the exciton binding energy to drive separation of colombically interacted holes and electrons.

Final and the next step of this working principle is the charge transportation and collection at the electrodes. After the free charges move toward the related electrodes, electrical circuit is completed. The impedance and the electrical conductivity of the semiconducting material play a crucial role in the charge transport and the device efficiency.^{58,61-63}

The operation principle of the organic solar cell is indicated in **Figure 23**.

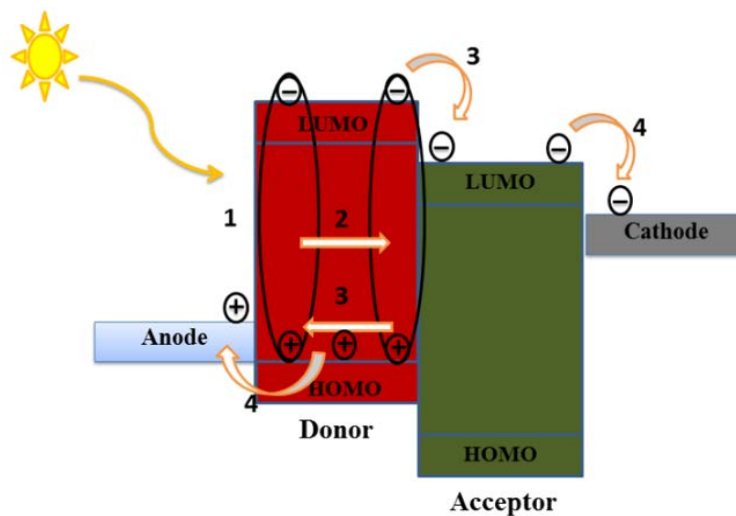


Figure 23. Working Principle of OSCs

1.10.2. Device Construction of Bulk Heterojunction OSCs

Device architecture of bulk heterojunction type organic solar cells composed of ITO/PEDOT:PSS(40nm)/Polymer:PC₇₀BM/LiF(0.6nm)/Al(100nm) in a given order. Schematic representation of bulk heterojunction type solar cell is demonstrated in **Figure 24**. Firstly, coating procedure of clean glass substrate with generally transparent conducting oxide like indium tin oxide (ITO) or transparent conducting layer like carbon nanotubes as the anode is performed. These type anodic materials are used due to its transparency and high work function ability to improve efficient hole injection. Onto the ITO surface, PEDOT:PSS as the protective hole transport layer is deposited through spin coated technique. PEDOT:PSS is the best choose in the literature to prevent electron migration to the anode. Additionally, this protective layer can improve transportation of photo generated holes from the active matrix to the anode. Active layer comprise from blend of synthesized conjugated polymer as donor and fullerene derivatives as acceptor is deposited between PEDOT:PSS via spin coated technique. Blend of donor and acceptor in the active material brings about reduction of exciton migration distance. Hence, bulk heterojunction solar cell shows higher power conversion efficiency when compared with single and bilayer organic solar cells. After that, LiF as electron transport layer is deposited on the active layer to improve electron transportation and block the holes. Finally, some metals, especially Al and Cu, are chosen as a cathode to collect generated electrons.⁵⁸

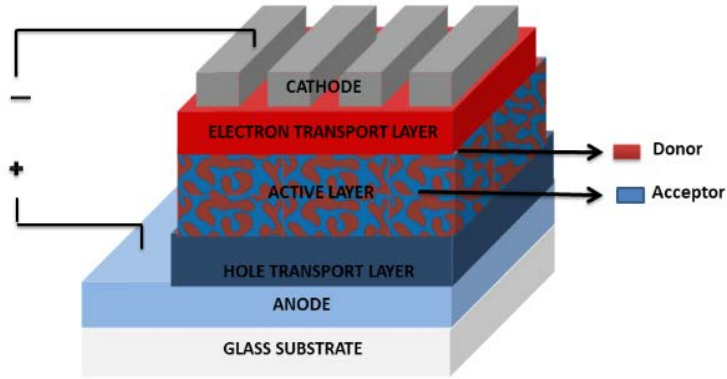


Figure 24. Device Architecture of Bulk Heterojunction OSCs

1.10.3. Characterization of an Organic Solar Cell Device

The current density-voltage (J-V) behavior of an organic solar cell in the dark and under illumination can be utilized to detect the organic solar cell performance at 25 °C. **Figure 25** shows the current density-voltage (J-V) curve of an organic solar cell in the dark and under illumination. In the case of dark, the organic solar cell behaves like a diode and the curves passes through the origin due to absence of almost no potential or current. By contrast, shifting of the J-V curve in the fourth quadrant is observed when the organic solar cell is illuminated. That is; the organic solar cell generates power. Basically, the ratio between P_{max} and P_{in} gives the PCE of the organic solar cell. The related equations is shown below **Eq. 2**.⁶⁴

$$PCE = \frac{P_{max}}{P_{in}} \quad P_{max} = V_{oc} * J_{sc} * FF \quad FF = \frac{J_{max} * V_{max}}{J_{sc} * V_{oc}} \quad \text{Eq.2}$$

Where, P_{in} is incident photon, P_{max} is maximum power, J_{sc} is short circuit current, V_{oc} is open circuit voltage and FF is fill factor.

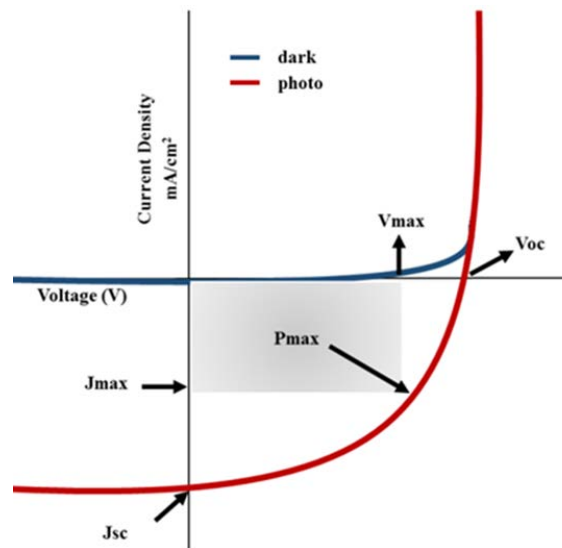


Figure 25. Current Density-Voltage (J-V) Graph of OSCs

Air Mass 1.5 Global (AM 1.5 G) with 1000 W/m^2 intensity is used as the standard illumination source in all the measurements of solar cell efficiency. Air mass describes the measurements of how much sunlight travels through the atmosphere to reach the surface of the earth with a defined angle. 1.5 in the AM 1.5 G term defines that sunlight reaches to the earth surface with an angle of 48° in a cloudless day.^{65,66} AM 1.5 G is illustrated in **Figure 26**.

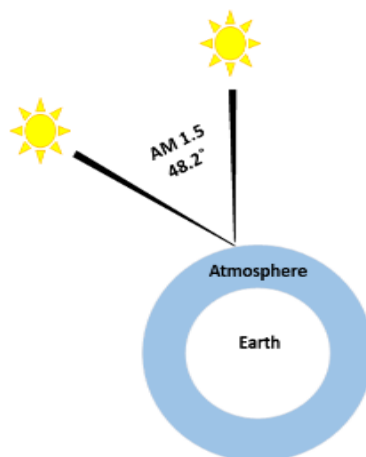


Figure 26. Illustration of AM 1.5 G

1.10.4. Important Parameters for OSC Efficiency

1.10.4.1. Open-Circuit Voltage (V_{oc})

Potential difference which arises across a photovoltaic cell is specified as the open circuit voltage (V_{oc}). Also, the energy difference between the HOMO level of the donor and the LUMO energy level of the acceptor moiety determines V_{oc} of the organic solar cell.^{60,61,67} In the organic solar cell, V_{oc} is directly or indirectly influenced by morphology of the active layer, light intensity, recombination of the exciton, interface area between donor and acceptor moiety, buffer layers between the electrodes and the active layer. According to many studies based on the improvement of the performance of an organic solar cell metal oxide or organic interfacial layer can hinder the electron transport at the anode. Therefore, V_{oc} and the PCE of the organic solar cell can be enhanced.^{68,69} The studies conducted by Scharber and coworkers reveal that the relationship between the V_{oc} and the energy difference of the donor-acceptor moieties in the bulk heterojunction solar cell.

$$V_{oc} = \left(\frac{1}{q}\right) [E(HOMO)_{donor} - E(LUMO)_{acceptor}] - 0.3 V \quad \text{Eq.3}$$

where q is the elementary charge (1.60×10^{-19} coulombs) and 0.3 V is related with the deviation from the achievable maximum V_{oc} .⁷⁰

1.10.4.2. Short-Circuit Current (J_{sc})

A solar cell produces maximum current during the absence of external resistance under illumination known as short-circuit current (J_{sc}). Small band gap, high absorption coefficient and high charge carrier mobility of an active layer can be contributed to obtain high J_{sc} . J_{sc} plays an important role to determine the PCE of the organic photovoltaic device. Additionally, there is a direct relation between the J_{sc} value and the external quantum efficiency (EQE). EQE can be described as the ratio of the

number of incident photon on a photovoltaic device to the number of collected charge carriers at the electrodes.⁷¹

1.10.4.3. Fill Factor (FF)

The another main parameter which affects the PCE of a photovoltaic device is the fill factor (FF). The relation between the transportation and recombination of the electron-hole pairs gives the FF value. FF shows tendency to decrease with the increasing of recombination of the charge carriers at the junction points and deviation of diode ideality is observed because of alteration of shunt and series resistance. In an ideal diode, shunt resistance (R_{sh}) and series resistance (R_s) should be infinity and zero, respectively. Reduction of the FF can be observed with the increasing of the R_s and therefore, deviation from ideal diode behavior can be obtained. If R_{sh} value reduces reduction in the current is observed owing to the arising of alternating current paths in the photovoltaic cell.

$$Fill\ Factor = \frac{J_{max} * V_{max}}{J_{sc} * V_{oc}} \quad \text{Eq.4}$$

where J_{max} and V_{max} are the maximum power point current density and the maximum power point current voltage, respectively.^{72,73}

1.11. Aim of the Study

Examples of the random copolymers with D-A terpolymer approach consisting of 2D-1A or 1D-2A units show relatively high light harvesting property in the literature. Random copolymerization with this approach is generally applied to enlarge absorption ability, adjust the molecular orbital energy by altering the composition of conjugated units in the copolymer and develop π - π^* transition between the polymer chains by designing proper copolymers having planar molecular structure.⁷⁴⁻⁷⁶ Due to the outstanding specialties of this random D-A terpolymer approach inventive two random copolymers comprising triphenylamine (TPA) and benzodithiophene (BDT)

derivatives as electron rich donor moieties and benzotriazole (BTz) with branch alkyl chain as electron deficient acceptor moiety have designed and synthesized via Stille coupling reaction. Furthermore, thiophene as conjugated linker was used due to its great optical and photovoltaic benefits. In this study, effect of bistriphenylamine and thiophene π -bridge on photovoltaic studies was mainly examined. Structures of these two conjugated polymers, **P1** & **P2**, were illustrated in **Figure 27**.

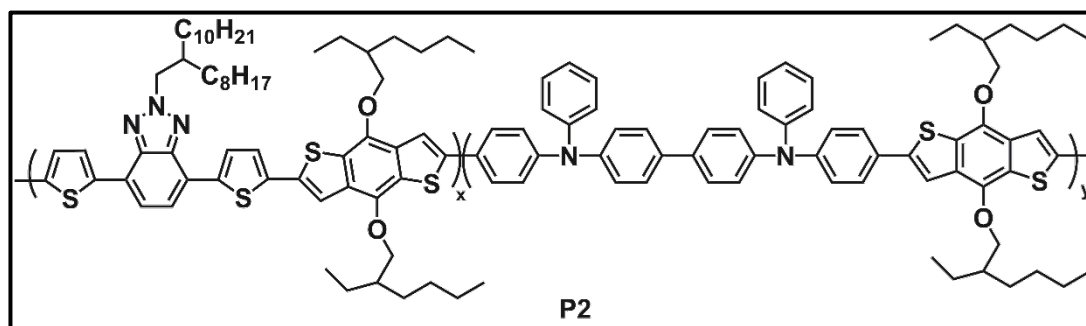
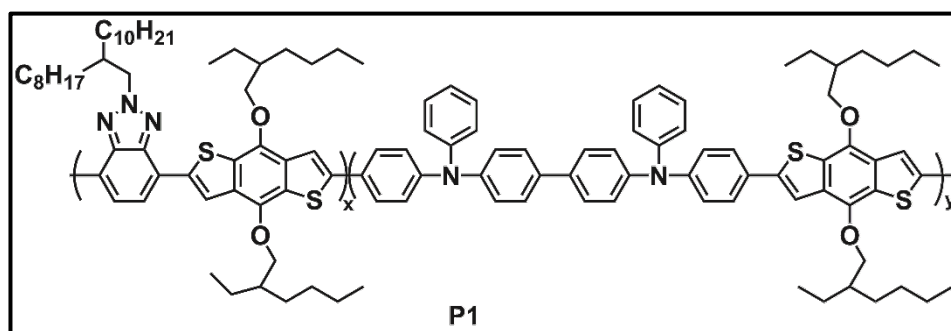


Figure 27. Structures of Synthesized **P1** and **P2**

CHAPTER 2

EXPERIMENTAL

2.1. General

All chemicals and solvents for the syntheses of polymers (**P1**, **P2**) were purchased from Sigma-Aldrich Co. Ltd. and used as received. 9-(Bromomethyl)nonadecane, tributyl(thiophen-2-yl)stannane, 4,7-dibromo-1H-benzo[d][1,2,3]triazole, 4,7-dibromo-2-(2-octyldodecyl)-2H-benzo[d][1,2,3]triazole, 4,7-bis(5-bromothiophen-2-yl)-2-(2-octyldodecyl)-2H-benzo[d][1,2,3]triazole (TBT) were synthesized with the same synthetic procedures reported in literature.^{33,77} Tetrahydrofuran (THF) was freshly distilled after drying over Na and benzophenone. Reactions were carried out under argon atmosphere. Structures of synthesized monomers and polymers were confirmed by nuclear magnetic resonance (NMR) spectra. ¹H and ¹³C spectra of the synthesized molecules in deuterated chloroform (CDCl₃) were recorded on a Bruker Spectrospin Avance DPX-400 Spectrometer by using trimethylsilane (TMS) as the internal reference. Number and weight average molecular weight of polymers were determined with gel permeation chromatography (GPC) on Polymer Laboratories GPC 220 using polystyrene as the reference and chloroform (CHCl₃) as the solvent. Electrochemical, spectroelectrochemical and colorimetry studies were performed by Gamry Reference 600 Potentiostat/Galvanostat and Varian Cary 5000 UV-Vis spectrophotometer, respectively. For electrochemical studies, a three electrode system which consists of a polymer coated indium tin oxide (ITO) as the working electrode, a Pt wire as the counter electrode and a Ag wire as the pseudo reference electrode. The electrolytic medium was 0.1 M tetrabutylammonium hexafluorophosphate (TBAPF₆)/acetonitrile (ACN) solution. Device architecture of

P1 and **P2** based organic solar cells are composed of ITO/PEDOT:PSS(40nm)/Polymer:PC₇₁BM/LiF(0.6nm)/Al(100nm) in a given order. Cleaning of ITO coated glass substrate was performed via toluene, detergent, distilled water and isopropyl alcohol during 15 min for each solvent in ultrasonic bath. After that, substrates were dried by nitrogen gun and cleaning procedure of them was continued with oxygen plasma for 5 min. Then, PEDOT:PSS coating was performed with spin-coating technique on precleaned ITO substrates thereafter baked at 135 °C for 15 min. In order to prepare **P1**:PC₇₁M and **P2**:PC₇₁BM blends in different weight to weight ratios *o*-DCB and CB were used, respectively. After these two blends were separately spin coated on PEDOT:PSS coated ITO substrates in N₂ filled glove box system, thermal evaporation of LiF /Al were carried out in the same system. In order to examine device performances current density-voltage (J-V) behavior of the devices were studied with Keithley 2400 source meter under 1.5 AM solar simulator while their incident photon to current efficiency (IPCE) performances were investigated with Oriel Quantum Efficiency Measurement Kit. Morphology of the active layer were investigated via atomic force microscopy (AFM) and transmission electron microscopy (TEM) analysis

2.2. Synthesis of Monomers

2.2.1. Synthesis of 9-(Bromomethyl)nonadecane

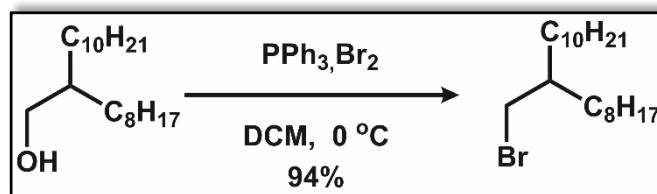


Figure 28. Synthetic Pathway of 9-(Bromomethyl)nonadecane

2-Octyl-1-dodecanol (5.00 g, 16.8 mmol) was dissolved in 20.0 mL DCM. Reaction was carried out at $0\text{ }^\circ C$. Then, triphenylphosphine (PPh_3) (4.63 g, 17.7 mmol) was added to the solution at that temperature. After PPh_3 addition was completed, bromine (Br_2) (2.82 g, 17.7 mmol) in 6.50 mL DCM was added to the reaction mixture dropwise and reaction medium was waited to reach room temperature. This mixture was stirred for 5 hours at room temperature. Then, slow addition of saturated solution of $NaHSO_3$ was performed to eliminate excess Br_2 . After get rid of excess Br_2 water was added to the reaction medium and extraction was performed with DCM. In order to obtain crude product as a colorless oil column chromatography on silica gel with hexane was performed (5.70 g, Yield: 94 %).

1H NMR (400 MHz, $CDCl_3$), δ (ppm): 3.38 (d, $J = 4.7$ Hz, 2H), 1.51 (m, 1.46-1.57 Hz, 1H), 1.23 (m, 1.15-1.32 Hz, 32H), 0.81 (t, $J = 6.58$ Hz, 6H). ^{13}C NMR (100 MHz, $CDCl_3$), δ (ppm): 39.5, 34.6, 32.5, 31.9, 31.6, 29.6, 29.3, 26.9, 26.5, 25.2, 22.7, 20.6, 14.1

2.2.2. Synthesis of 4,7-Dibromobenzo[c][1,2,5]thiadiazole

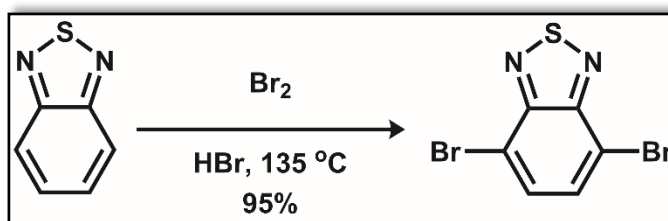


Figure 29. Synthetic Pathway of 4,7-Dibromobenzo[c][1,2,5]thiadiazole

Benzo-2,1,3-thiadiazole (5.00 g, 36.5 mmol) was dissolved in 50 mL (47%) HBr. After dissolving step, reaction was waited 10 minutes to reach room temperature. When reaction reached to room temperature Br₂ (17.5 g, 110 mmol) in 30 mL HBr was added gradually to the reaction medium. After Br₂ addition, reaction was refluxed overnight at 135 °C. Reaction was ended with TLC control and cooled to room temperature. Then, saturated solution of NaHSO₃ was added into the reaction medium and residue was filtered. This residue was washed many times with distilled water and cooled diethyl ether. 4,7-dibromobenzo[c][1,2,5]thiadiazole was obtained as yellow solid. (10.3 g, Yield: 96 %).

¹H NMR (400 MHz, CDCl₃), δ (ppm): 7.68 (s, 2H). ¹³C NMR (100 MHz, CDCl₃), δ (ppm): 152.94, 132.36, 113.91.

2.2.3. Synthesis of 3,6-Dibromobenzene-1,2-diamine

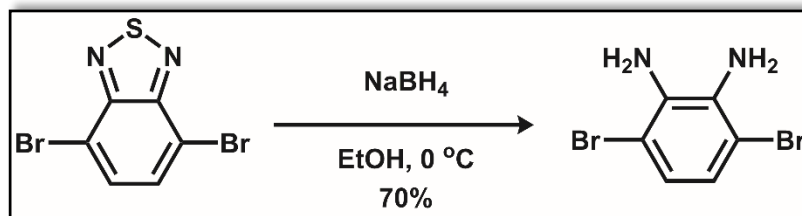


Figure 30. Synthetic Pathway of 3,6-Dibromobenzene-1,2-diamine

Firstly, 4,7-dibromobenzo[c][1,2,5]thiadiazole (5.20 g, 17.7 mmol) dissolved in 150 mL EtOH and the reaction mixture was put in an ice bath in order to reach 0 °C. After reaction mixture reached that temperature, slow addition of NaBH₄ powder (10.0 g, 266 mmol) was achieved to prevent rapid gas evolution. At the end of the gas evolution, this reaction medium was removed from the ice bath and waited to increase its temperature. Then, this mixture was stirred for 20 hours at room temperature. Later, evaporation of EtOH was completed under reduced pressure and orange residue was obtained. Water and brine were used many times to wash this residue. Finally, diethyl ether was evaporated from organic phase dried over MgSO₄ under reduced pressure to yield 3,6-dibromobenzene-1,2-diamine as a light yellow solid (3.29 g, Yield: 70 %).

¹H NMR (400 MHz, CDCl₃), δ (ppm): 6.85 (s, 2H), 3.91 (s, 4H). ¹³C NMR (100 MHz, CDCl₃), δ (ppm): 133.74, 123.26, 109.69.

2.2.4. Synthesis of 4,7-Dibromo-2H-benzo[d][1,2,3]triazole

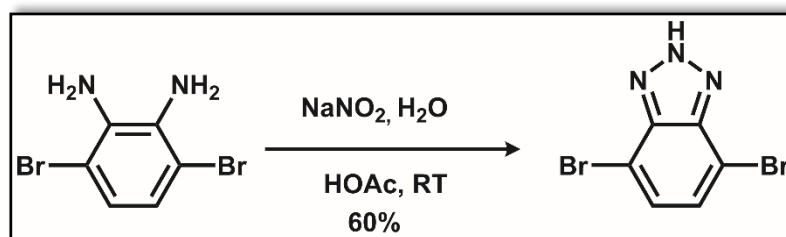


Figure 31. Synthetic Pathway of 4,7-Dibromo-2H-benzo[d][1,2,3]triazole

Firstly, dissociation of light yellow solid 3,6-dibromobenzene-1,2-diamine (3.29 g, 12.4 mmol) in 35 mL acetic acid (HOAc) and NaNO₂ (0.938 g, 13.6 mmol) in 20 mL distilled water were carried out. Then, NaNO₂ solution was added gradually into 3,6-dibromobenzene-1,2-diamine mixture. This mixture was stirred for 20 minutes at room temperature and residual formation in the reaction medium was observed. Then, filtration step was executed. The filtered solid was washed with distilled water several times to vanishe acid odor. Lastly, light yellow colored solid as a product was obtained (2.06g, Yield: 60 %).

2.2.5. Synthesis of 4,7-Dibromo-2-(2-octyldodecyl)-2H-benzo[d][1,2,3]triazole

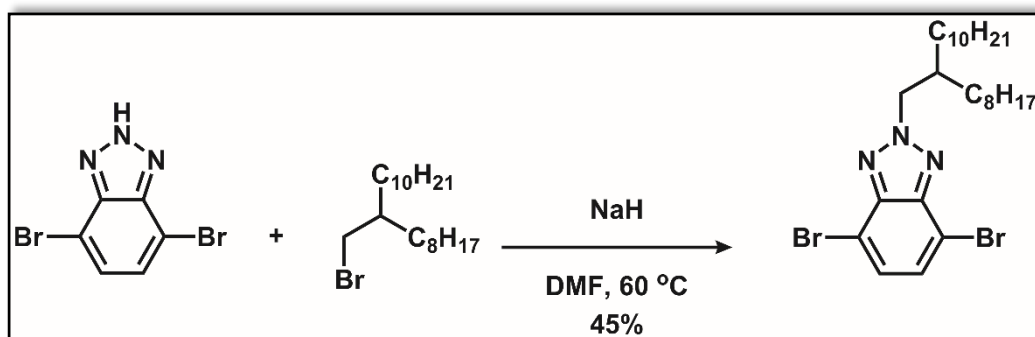


Figure 32. Synthetic Pathway of 4,7-Dibromo-2-(2-octyldodecyl)-2H-benzo[d][1,2,3]triazole

4,7-Dibromo-2H-benzo[d][1,2,3]triazole (2.06 g, 7.44 mmol) was dissolved in 10 mL anhydrous dimethylformamide (DMF) under Ar atmosphere and then, this mixture was put in an ice bath until its temperature dropped at 0 °C. Then, NaH (0.214 g, 8.93 mmol) was added into this reaction medium at that temperature. After NaH powders disappeared in the reaction medium this system was removed from the ice bath and heated to 60 °C. Then, 9-(bromomethyl)nonadecane was put in the system and stirred overnight. Reaction was terminated with TLC control. After vaporization of DMF under reduced pressure, product dissolved in CHCl₃ was washed many times by using distilled water and brine. Lastly, purification of 4,7-dibromo-2-(2-octyldodecyl)-2H-benzo[d][1,2,3]triazole was performed with column chromatography on silica gel (1:3 Hexane:CHCl₃) to yield pale yellow oil (1.87 g, Yield: 45 %).

¹H NMR (400 MHz, CDCl₃), δ (ppm): 7.28 (s, 2H), 4.58 (d, J = 7.2 Hz, 2H), 2.26 (m, 1H), 1.15 (m, 32H), 0.76 (m, 6H). ¹³C NMR (100 MHz, CDCl₃), δ (ppm): 141.00, 127.92, 108.01, 61.00, 38.2, 31.02, 30.91, 29.90, 29.06, 27.62, 27.53, 27.45, 27.32, 27.11, 26.98, 24.00, 22.10, 22.00, 13.11.

2.2.6. Synthesis of Tributyl(thiophene-2-yl)stanne

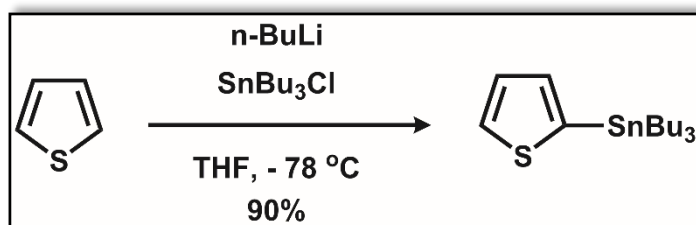


Figure 33. Synthetic Pathway of Tributyl(thiophene-2-yl)stanne

Thiophene (2.00 g, 23.8 mmol) was stirred for 10 minutes into a two neck round bottom flask under Ar atmosphere. After 10 mL anhydrous THF was put in the reaction system, bubbling with Ar was performed for 20 minutes. Then, temperature of the system was adjusted to -78 °C. When the reaction temperature dropped to this temperature n-buthyl lithium (n-BuLi) (2.5 M in hexane, 10.5 mL, 26.2 mmol) was added drop wise during 1.5 hours. After this addition was completed, the reaction mixture was stirred an additional hour at that temperature. Then, tributyltinchloride (SnBu₃Cl) (8.10 g, 25.0 mmol) was added slowly but faster than addition of n-BuLi in the reaction medium at -78 °C. This mixture was stirred overnight at room temperature. THF was evaporated from the reaction medium under reduced pressure. Cold water was put into the reaction and extraction was performed with diethyl ether. Finally, brown colored oil was obtained (7.99 g, Yield: 90 %).

¹H NMR (400 MHz, CDCl₃), δ (ppm): 7.57 (d, 1H), 7.20 (dd, 1H), 7.12 (d, 1H), 1.51 (t, 6H), 1.26 (dd, 6H), 1.05 (m, 6H), 0.83 (t, 9H).

2.2.7. Synthesis of 2-(2-Octyldodecyl)-4,7-di(thiophen-2-yl)-2H-benzo[d][1,2,3]triazole

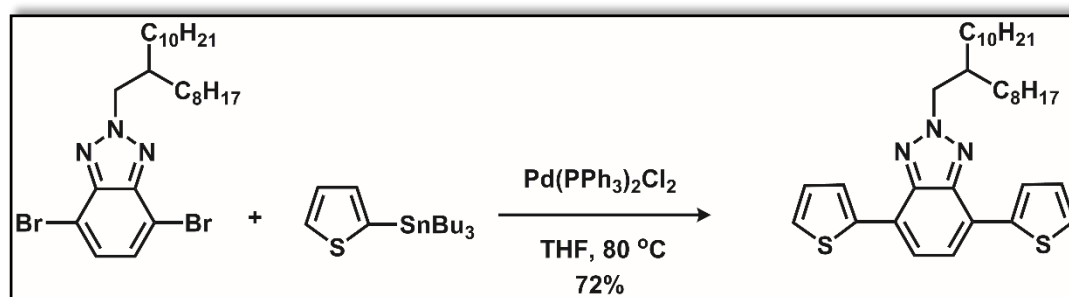


Figure 34. Synthetic Pathway of 2-(2-Octyldodecyl)-4,7-di(thiophen-2-yl)-2H-benzo[d][1,2,3]triazole

Ar was passed through the two neck round bottom flask which involved 4,7-dibromo-2-(2-octyldodecyl)-2H-benzo[d][1,2,3]triazole (1.00 g, 1.84 mmol) and tributyl(thiophen-2-yl)stanne (2.05 g, 5.50 mmol) for 20 minutes. After 15 mL anhydrous THF was put in the flask at room temperature, this system was stirred for half an hour under Ar atmosphere. Then, addition of bis(triphenylphosphine) palladium (II) dichloride (Pd(PPh₃)₂Cl₂) (96.9 mg, 0.138 mmol) was added into the reaction system. Temperature of the reaction was warmed up to approximately 80 °C and this mixture was refluxed overnight under Ar atmosphere. After this reaction was terminated by adding water, extraction was achieved with CHCl₃. Column chromatography technique on silica gel with hexane and DCM (4:1) was preferred in order to obtain pure 2-(2-octyldodecyl)-4,7-di(thiophen-2-yl)-2H-benzo[d][1,2,3]triazole as yellow solid (0.747 g, Yield: 72 %).

¹H NMR (400 MHz, CDCl₃), δ (ppm): 8.03 (dd, J = 3.6, 1.0 Hz, 2H), 7.56 (s, 2H), 7.30 (dd, J = 5.1, 1.0 Hz, 2H), 7.11 (dd, J = 5.1, 3.7 Hz, 2H), 4.68 (d, J = 6.6 Hz, 2H), 2.28 (m, 1H), 1.30 (dd, J = 12.4, 6.8 Hz, 7H), 1.17 (d, J = 9.3 Hz, 24H), 0.80 (m, 6H).

2.2.8. Synthesis of 4,7-Bis(5-bromothiophen-2-yl)-2-(2-octyldodecyl)-2H-benzo[d][1,2,3]triazole

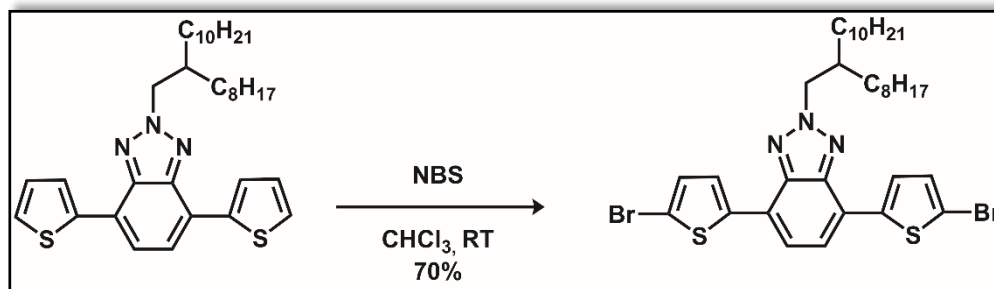


Figure 35. Synthetic Pathway of 4,7-Bis(5-bromothiophen-2-yl)-2-(2-octyldodecyl)-2H-benzo[d][1,2,3]triazole

Dissociation of 2-(2-octyldodecyl)-4,7-di(thiophen-2-yl)-2H-benzo[d][1,2,3]triazole (0.747 g, 1.32 mmol) was fulfilled in 20 mL CHCl₃. Then, N-bromosuccinimide (NBS) (0.587 g, 3.30 mmol) was added step wise within 1 hour into the reaction medium under dark condition at room temperature. This mixture was stirred overnight by continuing the dark condition at that temperature. After TLC control was performed, reaction was quenched with water. Extraction was fulfilled by using CHCl₃. In order to purify the product crystallization technique with EtOH was applied. Lastly, pure yellow solid 4,7-bis(5-bromothiophen-2-yl)-2-(2-octyldodecyl)-2H-benzo[d][1,2,3]triazole was collected (0.667 g, Yield:70 %).

¹H NMR (400 MHz, CDCl₃), δ(ppm): 7.71 (d, J = 4.0 Hz, 2H), 7.44 (s, 2H), 7.04 (d, J = 4.0 Hz, 2H), 4.66 (d, J = 6.6 Hz, 2H), 2.29 - 2.21 (m, J=6.0 Hz, 1H), 1.38 – 1.26 (m, 6H), 1.20 (d, J=8.2 Hz, 26H), 0.83 – 0.75 (m, 6H). ¹³C NMR (100 MHz, CDCl₃), δ (ppm): 141.75, 141.33, 127.52, 123.27, 121.79, 113.49, 62.00, 40.40, 32.28, 32.18, 31.78, 30.28, 29.98, 29.88, 29.68, 29.78, 24.60, 22.51, 14.4.

2.3. Synthesis of Polymers

2.3.1. Synthesis of P1

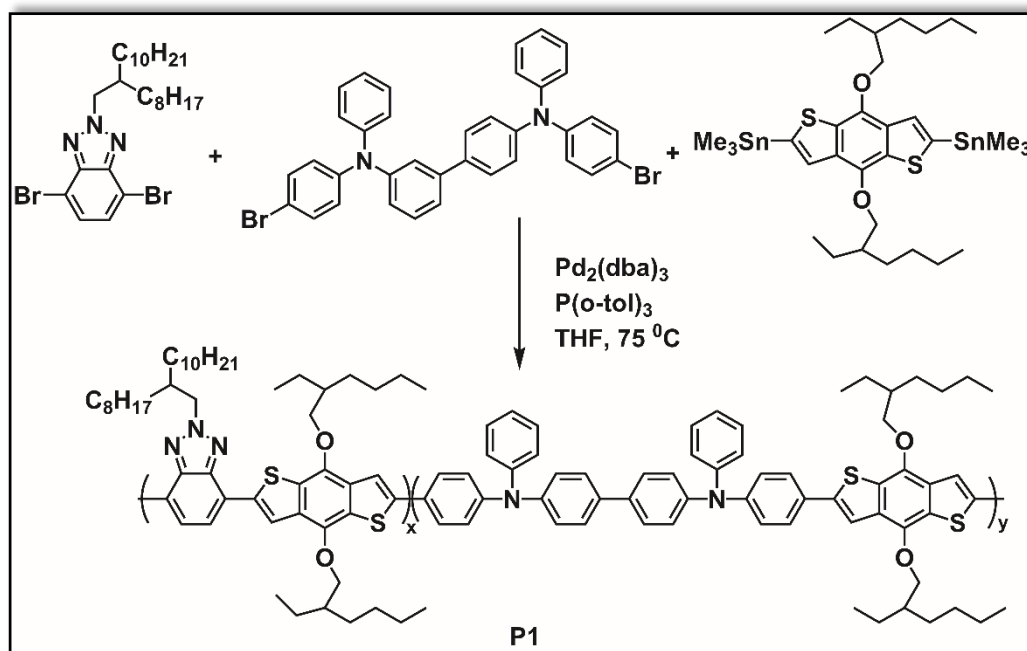


Figure 36. Synthetic Pathway of **P1**

4,7-Dibromo-2-(2-octyldodecyl)-2H-benzotriazole (64.6 mg, 0.116 mmol), 4,4'-bis[(4-bromophenyl)phenylamino]biphenyl (74.9 mg, 0.116 mmol) and 2,6-bis(trimethyltin)-4,8-bis(2-ethylhexyloxy)benzo[1,2-*b*:4,5-*b'*]dithiophene (179.0 mg, 0.232 mmol) were dissolved in 15 mL anhydrous THF in order to synthesize **P1** via Stille coupling reaction under Ar atmosphere. Then, bubbling with Ar was carried out for another 30 minutes. After bubbling step was finished, tris(dibenzylideneacetone)dipalladium (0) (10.6 mg, 0.0116 mmol) as catalyst and tris(*o*-tolyl)phosphine (7.10 mg, 0.0232 mmol) as co-catalyst were added into the reaction medium and the mixture was refluxed for 36 hours at 70 °C. Before the polymerization was ended, tris(dibenzylideneacetone)dipalladium (0) (5.30 mg,

0.00580 mmol) and tris(*o*-tolyl)phosphine (3.50 mg, 0.0116 mmol) were added to the reaction mixture. The reaction mixture was stirred at this temperature for 1 hour and bromothiophene (56.7 mg, 0.348 mmol) as the first end capper was added. Then, refluxed was continued at 70 °C for 5 hours. Addition of tributyl(thiophen-2-yl)stanne (260.0 mg, 0.695 mmol) as the second end capper was completed and reaction mixture was refluxed overnight. THF was removed under reduced pressure. The product was precipitated in cold methanol. Purification step was done with acetone and hexane via Soxhlet extractor. **P1** was extracted using CHCl₃. After evaporating CHCl₃ under reduced pressure, **P1** (171 mg, Yield: 83 %) as an orange-red colored end product was obtained. (GPC: M_n = 20 kDa, M_w = 50 kDa, PDI = 2.5)

¹H NMR (400 MHz, CDCl₃), δ (ppm): Aromatic: 8.66, 7.78–6.82, Aliphatic: 4.71 (N-CH₂): 4.50–3.70 (O-CH₂): 2.64–2.45, 2.05–0.83, 0.75.

2.3.2. Synthesis of P2

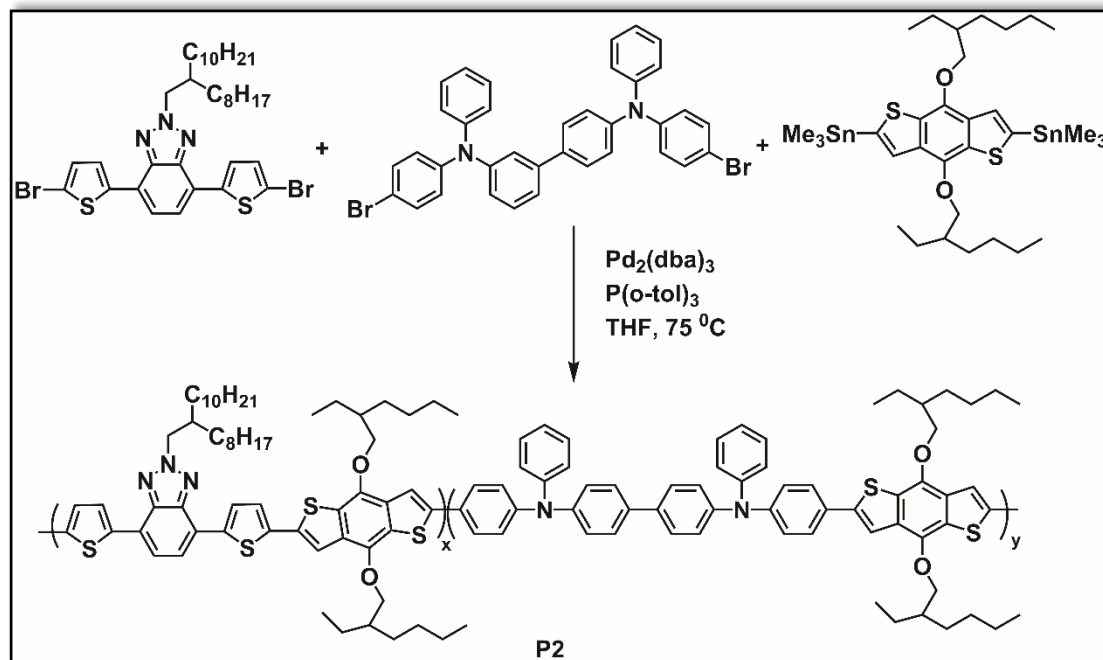


Figure 37. Synthetic Pathway of **P2**

Same synthetic route with **P1** was used to get **P2**. In order to achieve synthesis of **P2**, 4,7-bis(5-bromothiophen-2-yl)-2-(2-octyldodecyl)-2H-benzotriazole (83.0 mg, 0.115 mmol), 4,4'-bis(4-bromophenyl)phenylamino]biphenyl (74.3 mg, 0.115 mmol) and 2,6-bis(trimethyltin)-4,8-bis(2-ethylhexyloxy)benzo[1,2-*b*:4,5-*b'*]dithiophene (177.6 mg, 0.230 mmol) were dissolved in 15 mL dry THF under Ar atmosphere. After bubbling step was finished, catalyst and co-catalyst (tris(dibenzylideneacetone)dipalladium (0) (10.5 mg, 0.0115 mmol) and tris(*o*-tolyl)phosphine (7.10 mg, 0.023 mmol)) were added into the reaction mixture, respectively. Then, this reaction medium was refluxed for 36 hours at 70 °C under Ar atmosphere. Tris(dibenzylideneacetone)dipalladium (0) (5.70 mg, 0.0057 mmol) and tris(*o*-tolyl)phosphine (4.00 mg, 0.012 mmol) were added in the reaction mixture. The reaction mixture was stirred at 70 °C for 1 hour and bromothiophene (56.2 mg, 0.345 mmol) as the first end capper was added. Then, the reflux was continued at that

temperature for 5 hours. Addition of tributyl(thiophen-2-yl)stanne (257 mg, 0.690 mmol) as the second end capper was completed and the mixture was refluxed overnight. The product was precipitated in cold methanol. Purification step was fulfilled with acetone and hexane. **P2** was extracted with CHCl₃. After evaporation of CHCl₃ under reduced pressure, **P2** (140 mg, Yield: 80 %) as an orange-red colored end product was obtained. (GPC: M_n = 17 kDa, M_w = 39 kDa, PDI = 2.3)

¹H NMR (400 MHz, CDCl₃), d (ppm): Aromatic: 8.02, 7.79–6.69, Aliphatic: 4.70 (N-CH₂): 4.13 (O-CH₂): 2.53, 2.02–0.83, 0.77.

2.4. Characterization of Conjugated Polymers

2.4.1. Gel Permeation Chromatography

Gel permeation chromatography (GPC) is commonly preferred analytical separation technique in which identification of the molecular weight of macromolecules is performed according to size exclusion. GPC consists of porous, crosslinked polystyrene beads as stationary phase and liquid mobile phase which flows over these beads. Elution of smaller polymer chains from column is late compared to that of larger ones due to great entering fraction of small chain into the porous beads. Therefore, molecular weight and polydispersity index (PDI) of polymers (4 mg/2 mL) in a solvent such as CHCl₃, toluene, THF can be easily determined by refractive index detector.

2.4.2. Electrochemical Studies

Electrochemical properties of conjugated polymers are very crucial for usage in optoelectronic systems. With this aim, cyclic voltammetry (CV) as a three electrode system is practical and forceful way to investigate not only doping behavior but also positions of HOMO/LUMO energy levels. Therefore, electronic band gap is estimated depending upon difference between determined HOMO and LUMO energy levels. Working electrode (ITO), reference electrode (Ag wire), counter electrode (Pt wire) and voltage source (potentiostat) constitute this simple CV method.

In this study, spray coated conducting polymer on ITO-glass electrode was immersed into quartz cuvette where there is 0.1 M tetrabutylammonium hexafluorophosphate (TBAPF₆)/acetonitrile (ACN) electrolyte solution. During application of potentials supplied from potentiostat in proper range oxidation/reduction potentials, colors and redox feature of the polymer were determined with respect to single scan voltammogram.

2.4.3. Spectroelectrochemical Studies

Electrochemical analysis incorporated with UV-Vis-NIR spectral method is utilized to investigate wavelengths which maximum absorption takes place and polaron and bipolaron regions during incrementally increased potentials. Furthermore, optical band gap is confirmed by using onset value of maximum absorption wavelength.

In order to investigate spectroelectrochemical behavior of conjugated polymer ITO-glass slides coated with the polymer was put into 0.1 M TBAPF₆/ACN electrolyte solution. Then, Ag and Pt wires, namely reference and counter electrode, were attached to that slide and oxidation of the polymer's thin film was performed via stepwise raising potentials from potentiostat. UV-Vis-NIR spectroscopy allowed monitoring absorption spectra of the polymer during oxidation process.

2.4.4. Kinetic Studies

Percent transmittance change (% T) between fully oxidized and reduces state of thin film of polymer at maximum absorption wavelengths of neutral, polaron, bipolaron regions is designated via UV-Vis-NIR spectrometry and potentiostat. Additionally, needed time for polymer to reach completely its oxidized state from reduced state known as switching time is calculated. For these purposes, thin film of polymer into three electrode and electrolyte solution system cuvette was exposed to square wave potentials and transmittance against time graph was plotted via UV-Vis-NIR spectrometry during the same time.

2.4.5. Thermal Analysis

Thermal features of materials become very momentous parameter if these materials are used in optoelectronic systems since thermal stability of them affects the stability and lifetime of optoelectronic devices. Differential scanning calorimetry (DSC) and

thermal gravimetric analysis (TGA) are largely preferable thermal analysis techniques for polymers. While temperature was swept between a proper range to polymers via temperature controlling program of Perkin Elmer Differential Scanning Calorimetry heat capacity change (ΔC_p), glass transition temperature (T_g) and melting temperature (T_m) of the conjugated polymers were determined. Furthermore, decomposition temperature (T_d) and weight loss of the polymers were investigated with Perkin Elmer Pyris 1 Thermal Gravimetric Analysis instrument after stepwise heating was performed.

2.4.6. Photovoltaic Studies

Etching process was applied to surface of glass substrates coated with ITO by immersing in HCl and HNO₃ solution. After etching took 3 minutes, cleaning step of etched these substrate was performed with toluene, detergent (Hellmanex III), water acetone, isopropanol in ultrasonic bath. This process was last 15 minutes for each cleaner. Then, N₂ gun was utilized to dry surface of the cleaned substrates before oxygen plasma treatment as a last step was applied via Harrich Plasma Cleaner. After all of the cleaning steps were completed, device fabrications of these polymers were constructed with ITO coated glass substrate, PEDOT:PSS (40 nm), (**P1** or **P2**):PC₇₁BM, LiF (0.6 nm) and Al (100 nm) in a given order. With this aim, PEDOT:PSS filtered with 0.45 μ m PVDF filter was coated on the ITO-glass substrates with spin coating technique. In order to remove water from covered part with PEDOT:PSS drying was carried out at 130 °C for 20 minutes since PEDOT:PSS involved water. After then, **P1** or **P2** and PC₇₁BM mixtures in different weight ratios filtered with PVDF filter and spin coating of these mixtures on PEDOT:PSS were successfully performed under nitrogen atmosphere in glove box system. Later on, coating of LiF and Al on **P1** or **P2**:PC₇₁BM layer was performed by evaporating. Photovoltaic properties as current density-voltage relation of the constructed devices was examined by using Keithley 2400 source meter under AM 1.5 G solar simulator of Atlas Material Testing Solutions.

CHAPTER 3

RESULTS & DISCUSSION

3.1. Electrochemical Studies

Redox features of random copolymers were examined with cyclic voltammetry (CV) in 0.1 M tetrabutylammonium hexafluorophosphate/acetonitrile (TBAPF₆/ACN) electrolyte solution to reveal doping behaviors, HOMO-LUMO energy levels and electronic band gaps of the polymers. For this purpose, copolymers were dissolved in chloroform solution (5mg mL⁻¹) and spray coated on the ITO working electrodes and studies were performed with 100 mV s⁻¹ scan rate.

Electronic features of two copolymers were demonstrated in **Table 1**. Both polymers possess p and n doping characters as given in **Figure 38**. Doping and dedoping potentials of **P1** during p-type doping are 1.09 V/0.76 V. Furthermore, **P1** has two reversible redox couples during n-type doping centered at -1.72 V, / -1.63 V and -1.99 V/ -1.94 V. Doping/dedoping peak potentials of ambipolar **P2** at both p and n-doped sites were determined as 0.96 V/0.60 V and -1.75 V/-1.62 V. The different oxidation and reduction potentials of the polymers can be attributed to the varied electron distribution on the polymer backbone. When redox potentials of **P1** are compared with those of **P2**, **P2** has lower redox potentials since main backbone of **P2** chains incorporate electron rich thiophene as π -conjugated linker.

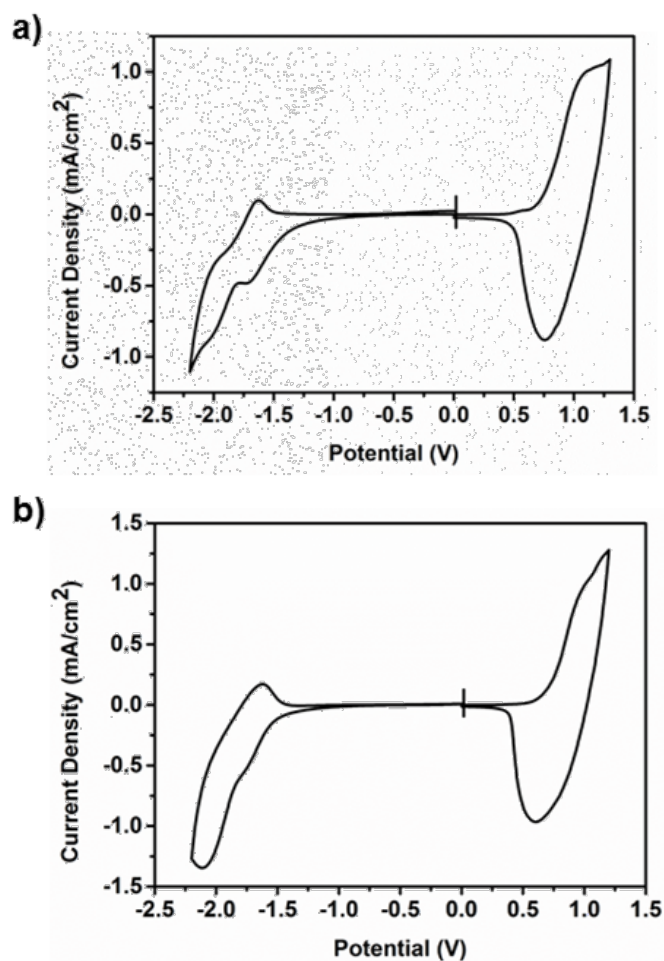


Figure 38. Single Scan Cyclic Voltammograms of **P1** (a) and **P2** (b) in 0.1 M TBAPF₆/ACN Electrolyte Solution at 100 mV s⁻¹ Scan Rate

Owing to ambipolar features of **P1/P2**, both HOMO and LUMO energy levels were determined using corresponding onset potentials according to **Eq. 5a, 5b**. In this equation, -4.75 eV value was taken as standard hydrogen electrode redox potential value.

$$\text{HOMO} = - (4.75 + E_{ox}^{onset}) \quad \text{Eq. 5a}$$

$$\text{LUMO} = - (4.75 + E_{red}^{onset}) \quad \text{Eq. 5b}$$

While HOMO and LUMO energy levels for **P1** were calculated as -5.47 eV and -3.41

eV, those of **P2** were estimated as -5.43 eV and -3.27 eV, respectively. HOMO energy level of **P2** is relatively higher than that of **P1** which can be explained with higher electron density of **P2** due to presence of thiophene unit on the main backbone. Electronic band gaps for **P1** and **P2** are similar due to difference between their HOMO and LUMO energy levels.

Table 1. Results of Electrochemical Studies of **P1** and **P2**

	$E_{p-doping}$ (V)	$E_{p-dedoping}$ (V)	$E_{n-doping}$ (V)	$E_{n-dedoping}$ (V)	HOMO (eV)	LUMO (eV)	E_g^{el} (eV)
P1	1.09	0.76	-1.72/ -1.99	-1.63/ -1.94	-5.47	-3.41	2.06
P2	0.96	0.60	-1.75/ -2.10	-1.62	-5.43	-3.27	2.16

3.2. Spectroelectrochemical Studies

Spectroelectrochemical studies of polymers were carried out via gradually increasing potential in 0.1 M TBAPF₆/ACN to find out optical features such as maximum absorption behaviors of polymers and optical band gaps. Polymers with 5 mg mL⁻¹ in CHCl₃ were spray coated on ITO coated glass substrate. **P1** was subjected to cycling between 0.0 V and 1.3 V where **P2** was recorded between 0.0 V and 1.2 V.

Maximum absorption range of the polymers are illustrated in visible range as reported in **Figure 39**. Similar to the most of the D-A type conjugated polymers, both polymers have two maximum absorption maxima (λ_{max}) due to $\pi-\pi^*$ transitions on the polymer main backbone and intermolecular charge transfer between donor and acceptor blocks.⁷⁸ While these two peaks for **P1** were recorded at 527 nm and 488 nm, absorption peaks of **P2** were observed at 481 nm and 416 nm.

Absorption band observed at neutral state was waned gradually with the formation of

absorption bands of polarons and bipolarons (**Figure 39**). In polaron and bipolaron regions, maximum absorptions were recorded at 730/1490 nm for **P1** and 715/1480 nm for **P2**. Optical band gaps (E_g^{op}) were calculated as 2.16 eV for **P1**, 2.11 eV for **P2** using 574 nm and 588 nm as the onset wavelength values respectively. All spectroelectrochemical results are shown in **Table 2**.

$$E_g^{op} = \frac{1241}{\lambda_{onset}} \quad \text{Eq. 6}$$

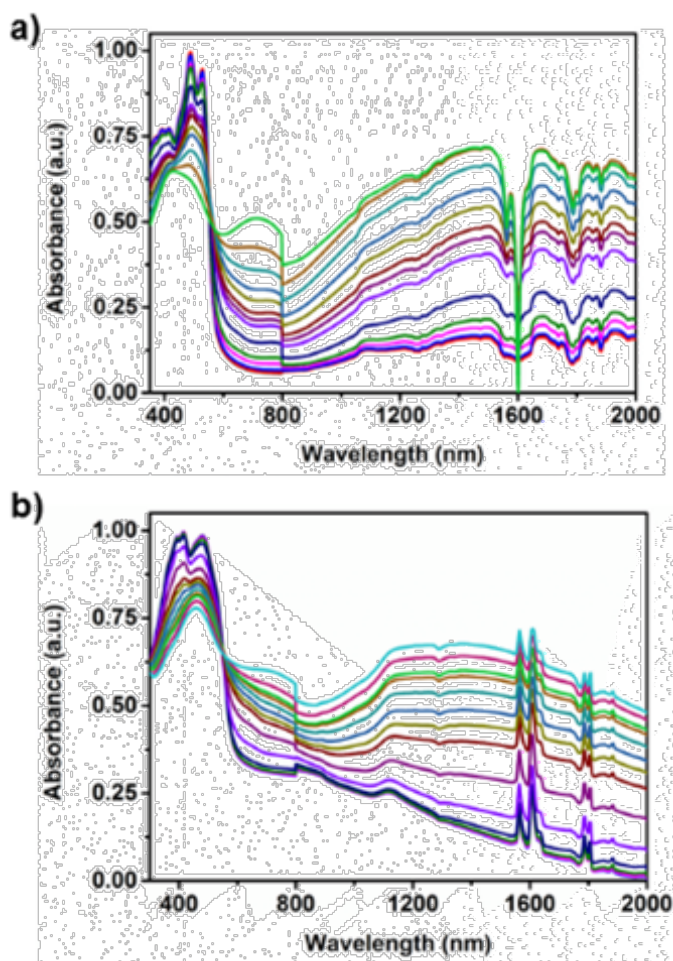
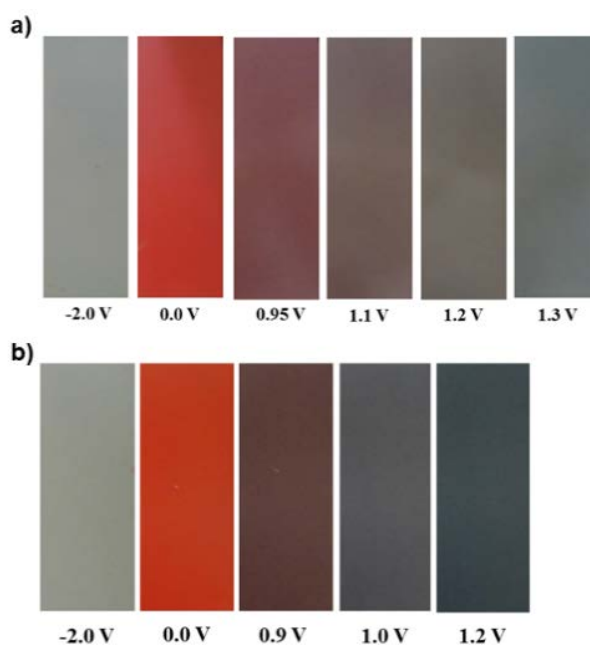


Figure 39. Electronic Absorption Spectra of **P1** (a) and **P2** (b) in 0.1 M TBAPFA6/ACN Electrolyte Solution

Table 2. Results of Spectroelectrochemical Studies of **P1** and **P2**

	λ_{\max} (nm)	E_g^{op} (eV)
P1	527/488	2.16
P2	481/416	2.11



		0.0	0.95	1.1	1.2	1.3	-2.0
		V	V	V	V	V	V
P1	L	40	38	41	12	46	61
	a	43	19	7	1	-2	-2
	b	32	5	3	5	-1	0

		0.0	0.9	1.0	1.2	-2.0
		V	V	V	V	V
P1	L	44	29	37	30	60
	a	52	12	0	-3	-2
	b	47	9	-1	-4	4

Figure 40. The Colors of **P1** (a) and **P2** (b) upon Oxidation and Reduction with Their L, a and b Value

Colors of the polymers shown in **Figure 40** were identified via International Commission on Illumination (CIE) system depending upon L (luminance), a (hue) and b (saturation) values of the polymers. While L value is corresponding to color's brightness, a and b are related with the color between red-magenta-blue and blue-yellow, respectively. Both polymers show multichromic behavior.

P1 and **P2** possess almost similar colors at their neutral, intermediate and fully oxidized states. Former has orange red color at neutral state, red and gray tones as intermediate colors and greenish gray color at fully oxidized state. Both polymers show light blue colors at -2.0 V.

3.3. Optical Studies

As illustrated in **Figure 41**, red shift features in the absorption were investigated for the thin films of the polymers compared to polymer solutions in chloroform. Absorption peaks of **P1** in thin film were examined at 488 and 527 nm but **P1** in CHCl_3 solution exhibited a peak at 483 nm. In the same manner, absorption wavelengths of **P2** in thin film form were recorded at 416 nm and 481 nm. Whereas, 466 nm was the value for **P2** in CHCl_3 . The reason of this phenomenon is related with absence of pre-aggregation effect, increasing delocalization of π -electrons with planar solid state, interaction between solvent-polymer and facilitating π - π^* transitions with diminished rotational angles in the polymer backbone.⁷⁹⁻⁸¹

Normally, optical absorption of **P2** is red shifted compared with that of **P1** due to the presence of higher electron density thiophene spacer on main polymer backbone. Entity of π -bridges such as thiophene, thiono[3,2-*b*]thiophene etc. strongly influences the electronic and optical behaviors of polymers with increasing planarity, intermolecular π - π stacking and electron delocalization ability. Additionally, conjugation length can also affect the optical properties of the polymers.⁸² According to optical absorption results of the polymers, **P1** has a more red shifted behavior. The reason of this unexpected result could be ascribed to the shorter conjugation length of **P2** due to lower molecular weight. That is; lower molecular weight of **P2** contributed

to short conjugation length, thereby causing this unforeseeable blue shift. Owing to the blue shifted property of **P2** this polymer has a deeper orange color compared to that of **P1**.

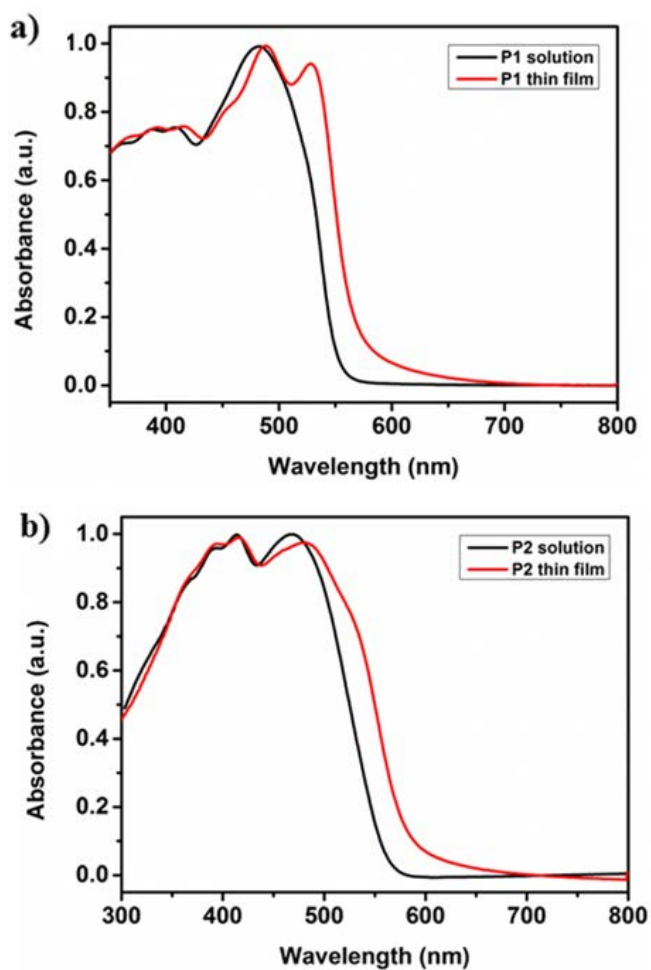


Figure 41. Normalized Absorption Spectra of **P1** (a) and **P2** (b) in Thin Film and CHCl_3 Solution

3.4. Kinetic Studies

In kinetic studies, percent transmittance change ($\Delta T\%$) and switching time behaviors

of the polymers between neutral and completely oxidized states were examined. Switching time can be defined as the time needed for observing the color switching of the electrochrome via oxidation and reduction processes. During kinetic studies, UV-Vis-NIR spectrometry was used by introducing square wave potentials within proper time intervals to the polymers at maximum absorption wavelengths which were chosen from the neutral, polaron and bipolaron absorption regions in the spectroelectrochemical results. With this aim, **P1** and **P2** coated on ITO glass substrate were subjected to square-wave potentials during 5 seconds for each cycle.

Percent transmittance changes were recorded as 20% at 527 nm, 46% at 730 nm, 76% at 1490 nm for **P1** and 21% at 418 nm, 51% at 715 nm, 64% at 1480nm for **P2**. Switching time values of **P1** and **P2** were calculated as 0.9 s, 1.2 s, 1.9 s and 1.5 s, 0.8 s, 1.8 s at their corresponding wavelengths, respectively. All kinetic results were summarized in **Table 3**.

P1 illustrated higher performance than **P2** in accordance with these results. Expectedly, **P2** with thiophene should give better kinetic results since this spacer may enhance ion diffusion ability and dopant insertion by increasing the conjugation length.^{83,84} However, aforementioned lower molecular weight of **P2** might be the reason of rather worse kinetic values compared to **P1** since **P2** has a lower conjugation length. Therefore, ion diffusion and dopant insertion ability of **P2** were weak.²⁷

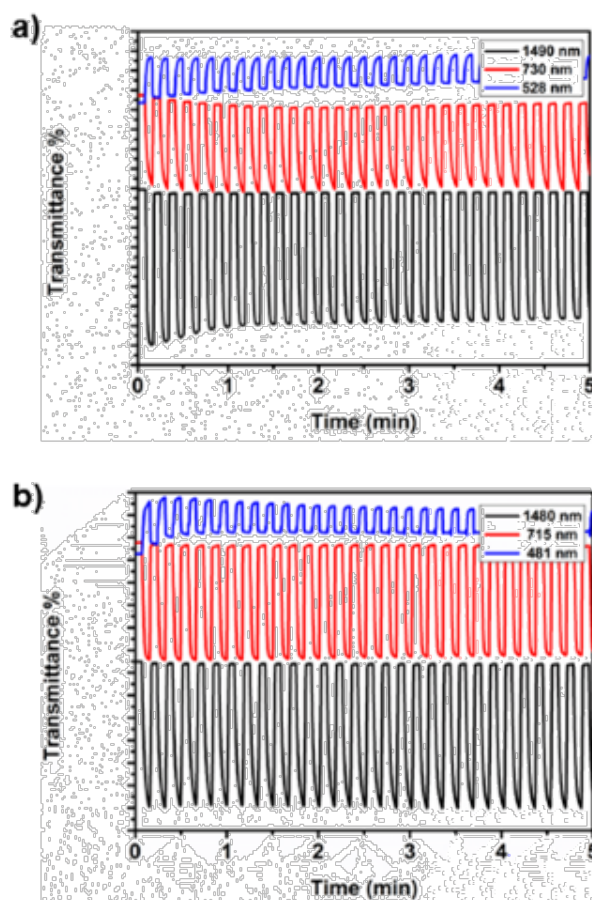


Figure 42. Percent Transmittance Change (ΔT %) of **P1** (a) and **P2** (b) in 0.1 M TBAPF₆/ACN Electrolyte Solution at Maximum Neutral, Polaron, Bipolaron Absorption Wavelengths

Table 3. Results of Kinetic Studies of **P1** and **P2**

	Wavelength (nm)	Transmittance (%)	Switching time (s)
P1	527	20	1.9
	730	46	1.2
	1490	76	0.8
P2	481	21	1.8
	715	51	0.8
	1480	64	1.5

3.5. Thermal Analyses of Polymers

Thermogravimetric and thermal features of the polymers were examined via thermal gravimetric analysis (TGA) and differential scanning calorimeter (DSC), respectively. According to DSC results of the polymers both of the polymers did not exhibit any glass transition temperature (T_g). Additionally, mass loss of the polymers was recorded as 50% at 600 °C for **P1** and 41% at 700 °C. That is; **P1** and **P2** revealed high thermal stability up to 350 °C. The results of DSC and TGA analyses were shown in **Appendix A**.

3.6. Organic Solar Cell Device Applications

The device architecture of bulk heterojunction polymer-based photovoltaic device was constructed as ITO/PEDOT:PSS/polymer:PC₇₁BM/LiF/Al. Efficiency of the organic photovoltaics was investigated by applying some optimization studies under AM 1.5 G illumination source. These optimized studies such as solvent selection, donor-acceptor ratio, active layer thickness, addition of additive and methanol treatments are the important and the most effective parameters in order to obtain high PCE of an organic solar cell. **Table 4** and **Table 5** summarize the effect of optimized studies to current density-voltage (J-V) behaviors of the polymer **P1** and **P2** based organic solar cell, respectively.

In this study, PC₆₁BM as an acceptor moiety was not selected instead of less symmetric PC₇₁BM since more symmetric fullerene derivative PC₆₁BM shows less light absorption ability and also, cannot enhance current density of the photovoltaic devices as much as less symmetric PC₇₁BM.⁸⁵

Table 4. Results of Photovoltaic Studies of **P1**

Polymer:PC₇₁BM	%	V_{oc} (V)	J_{sc} (mA/cm²)	FF (%)	PCE (%)	Active Layer Thickness (nm)
P1 (1:1)	2	0.78	5.43	42	1.77	109
P1 (1:2)	2	0.79	7.49	50	2.85	106
P1 (1:2)	3	0.79	9.45	47	3.50	124
P1 (1:2)	3	0.81	6.85	55	3.05	114
P1 (1:3)	2	0.72	5.65	44	1.80	99

Table 5. Results of Photovoltaic Studies of **P2**

Polymer:PC₇₁BM	%	V_{oc} (V)	J_{sc} (mA/cm²)	FF (%)	PCE (%)	Active Layer Thickness (nm)
P2 (1:1)	2	0.77	5.43	39	1.45	118
P2 (1:2)	2	0.75	8.59	49	3.15	112
P2 (1:2)	2	0.75	4.51	37	1.25	118
P2 (1:2)	2	0.76	6.66	38	1.89	125
P2 (1:3)	3	0.75	8.63	42	2.71	105
P2 (1:4)	3	0.75	7.66	44	2.52	100

In the bulk heterojunction type photovoltaics, blend of polymer as a donor purpose and fullerene derivatives as an acceptor purpose are used to enhance the PCE of the photovoltaic. In this case, weight ratio between the polymer and the fullerene based materials plays an important role to optimize the device and obtain high PCE since balance between charge transport and absorption of the active layer affect the performance of the photovoltaic.⁸⁶ Different polymer:PC₇₁BM weight ratio was applied to obtain high device performance and it was easily seen that the device efficiency improved when **P1** or **P2**:PC₇₁BM ratio was changed from 1:1 to 1:2 due to larger fill factor and current density value. When PC₇₁BM ratio was increased to 1:3 in the active layer device performance decreased because of becoming less predominant light harvesting ability of the polymers (**P1** and **P2**).⁸⁷

Device efficiency depends on morphology of the active layer as well as polymer:PCBM weight ratio. When bicontinuous and more interconnected donor-acceptor network were obtained PCE of the photovoltaic device was enhanced and high device performance was observed. 1,8 diiodooctane (DIO) addition is one of the most applied strategy to improve the morphology of the active layer of the organic solar cells by increasing the formation of more interconnected donor-acceptor domain network. Generally, only DIO addition is not enough for improvement of the morphology. Therefore, methanol (MeOH) treatment is applied to obtain stable and homogenous active surface.⁸⁸ Best device performance **P1** based photovoltaic device was recorded as 3.50% PCE, 0.79 V V_{oc} and 9.45 mA cm⁻² J_{sc} with 3% vol. DIO and MeOH treatments. After these treatments were used **P2** based photovoltaic device its efficiency suddenly reduced from 3.15% to 1.89%. In order to investigate the results of the reduction in PCE of **P2** with applied treatments, atomic force microscopy (AFM) and transmission electron microscopy (TEM) analysis were applied to the active layers of the photovoltaics (**Figure 43** and **Figure 44**). Additionally, active layer thickness was an important parameter for high PCE and the thickness was determined via AFM studies. Results of the thickness study were shown on **Table 4** and **Table 5**. In TEM images, bright and dark regions are associated with polymers and PCBM rich domains, respectively. According to TEM images of the polymer and PC₇₁BM blend with/without treatments, **P2** based device shown poor interconnected donor-acceptor

domain network compared with the **P2** based device without DIO/MeOH treatment. The highest power conversion efficiency of the **P2** based organic solar cell was determined as 3.15% with 0.75 V of V_{oc} and 8.59 mA cm^{-2} of J_{sc} . The device performance of **P1** and **P2** based organic photovoltaics was calculated using J-V graph of the devices. **Figure 45** belongs to the J-V graph of the best performance solar cells.

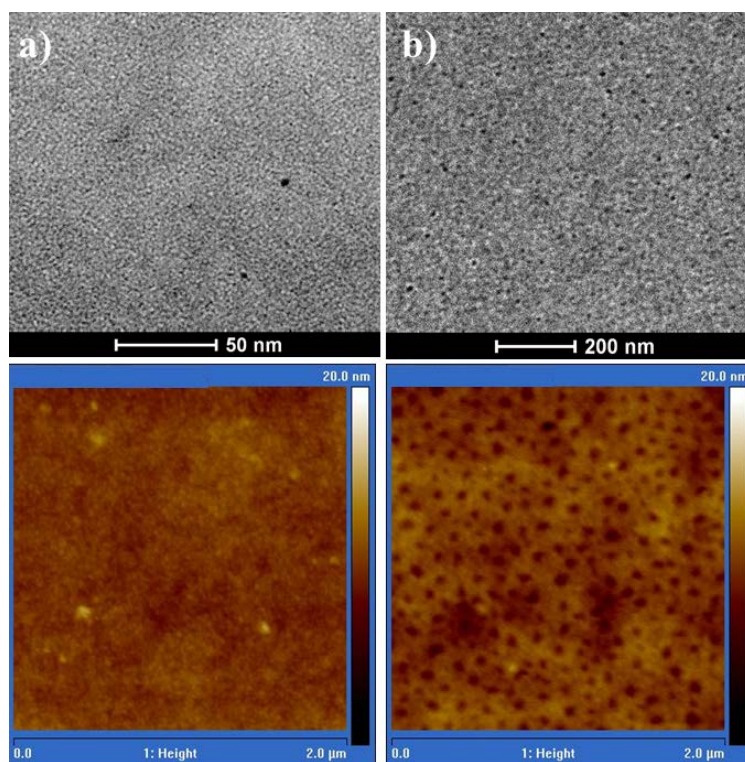


Figure 43. TEM and AFM Images of **P1:PC₇₁BM** (1:2 w/w) blend without treatment (a) with treatment (b). (Scale bars are 250 nm.)

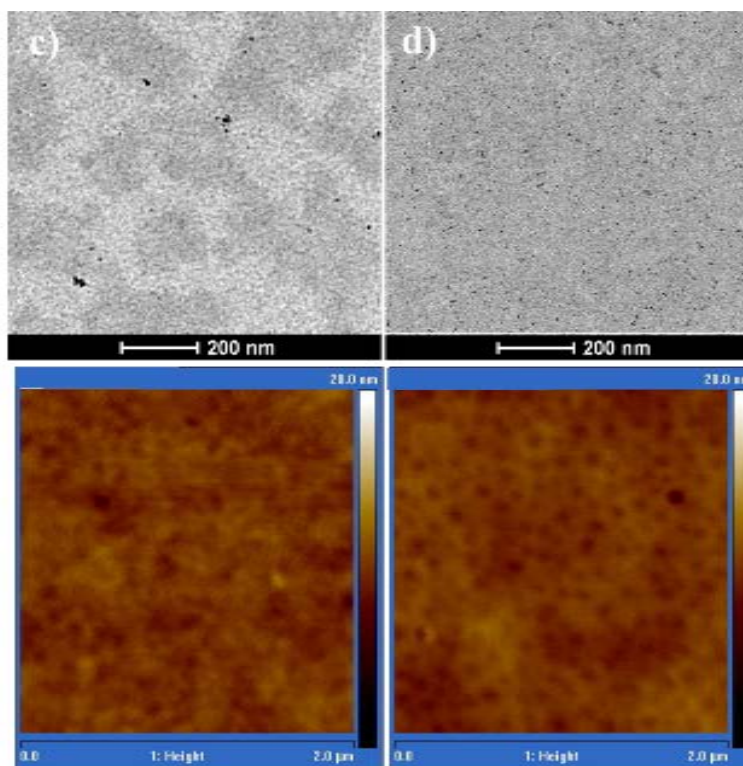


Figure 44. TEM and AFM images of **P2**:PC₇₁BM (1:2 w/w) blend without treatment (c) with treatment (d). (Scale bars are 250 nm.)

Low HOMO energy levels of **P1** and **P2** brought about high V_{oc} value for the photovoltaic devices. V_{oc} values of **P1** and **P2** based devices were changed between 0.72-0.81 V and 0.75-0.77 V, respectively. Additionally, J_{sc} values of the **P1** and **P2** were very close to each other. However, FF values of **P1** were much better compared with FF value of **P2**. While FF values of **P1** varied between 47-55% FF results were recorded between 39-44% for **P2** based devices.

Although **P1** and **P2** exhibited similar electronic and optical behaviors **P1** possessed higher photovoltaic performance compared with **P2** device performance. Higher molecular weight (M_n) value of **P1** may be the reason of this phenomenon since high M_n value of the polymer can led to more charge carrier mobility. M_n value of **P1** and **P2** were recorded as 20 kDa and 17 kDa, respectively.

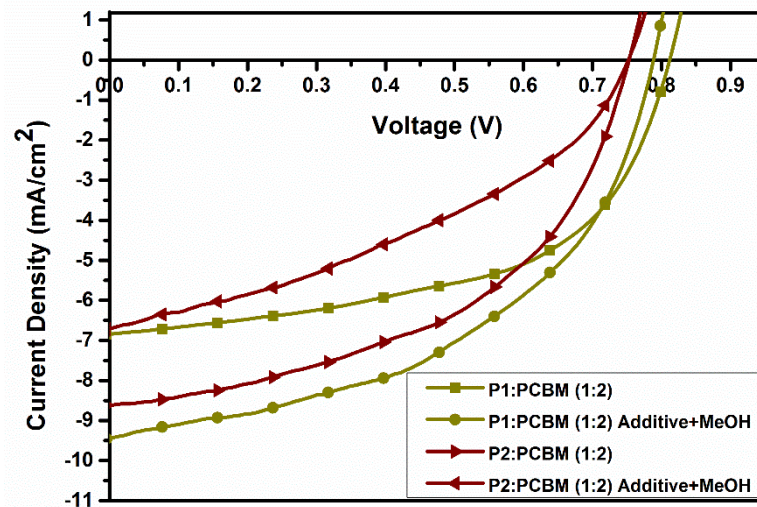


Figure 45. Current Density-Voltage (J-V) Behavior of **P1** and **P2** Based Best Performance Devices

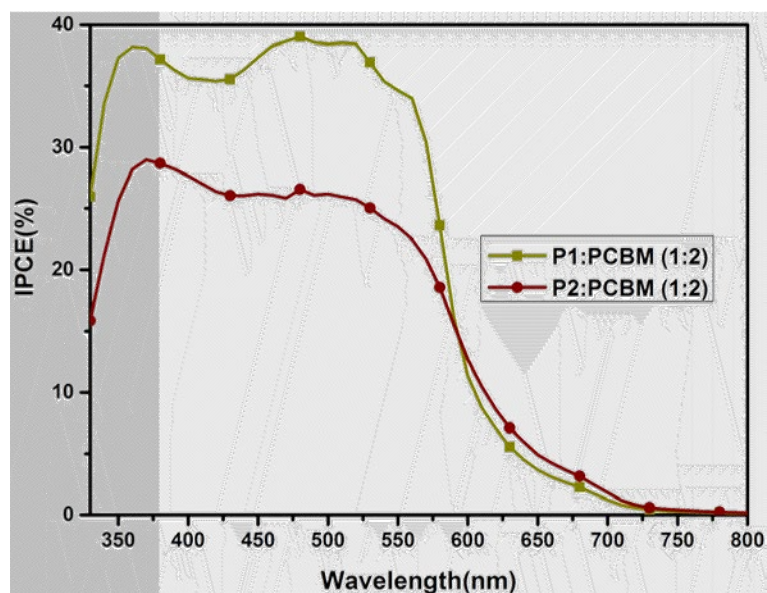


Figure 45. IPCE Curve of **P1:PC₇₁BM** (1:2 w/w) blend with treatment and **P2:PC₇₁BM** (1:2 w/w) blend without treatment based organic solar cells

The ratio of number of charges collected by electrodes to the number of incident photons can be expressed with incident photon to current efficiency (IPCE) study. **Figure 45** shows IPCE curves of the best performance **P1** and **P2** based devices. According to IPCE measurements 39% and 28% photocurrent values were recorded for best performance **P1** and **P2** based devices, respectively. Lower photocurrent results of **P2** can be related with the increment of recombination center owing to lower Mn value of **P2** and lower J_{sc} value compared with **P1**.^{89,90} IPCE values were calculated according to **Eq. 7**.

$$IPCE = \frac{1241 * J_{sc}}{\lambda * P_{in}} \quad \text{Eq. 7}$$

Where J_{sc} is short circuit current, λ is wavelength of incident light and P_{in} is incident photon.

CHAPTER 4

CONCLUSIONS

Syntheses of the D-A type conjugated random copolymers comprising BTz, bistrisphenylamine and BDT were achieved successfully via Stille coupling reaction to examine optical, electronic, and optoelectronic behavior of the polymers. They demonstrated proper electrochemical, spectroelectrochemical, and optical behaviors for photovoltaic applications. They showed not only proper film forming performance but also high thermal stability up to 350 °C. Neutral state color of **P1** was orange-red whereas **P2** exhibited darker orange color its neutral state due to blue shifted absorption for low molecular weight **P2**. The polymers showed ambipolar character and their frontier energy levels were calculated as 25.47 eV/ -3.41 eV for **P1** and 25.43 eV/-3.27 eV for **P2** using CV. Maximum absorptions of **P1** were recorded at 527 nm/488 nm while **P2** exhibited two maximum absorptions at 481 nm/416 nm. This blue shifted absorption behavior of **P2** compared to absorption feature of **P1** can result from shorter conjugation length of **P2**. The difference between HOMO level of **P1** and LUMO level of PC₇₁BM is lower than that of **P2**. This results in generally lower V_{oc} values of constructed cell with **P2**. Inclusion of thiophene p-bridge makes low lying HOMO and LUMO levels which reduce the V_{oc} . The reduced V_{oc} of **P2** with low photocurrent ends up with lower PCE values. Furthermore, the highest PCE of OSC based on **P1**:PC₇₁BM (1:2 w/w) in 3% o-DCB solution was recorded as 3.50% with DIO addition and methanol treatment. This device also revealed V_{oc} ; 0.79 V, J_{sc} ; 9.45 mA cm⁻², FF; 53%. **P2**:PC₇₁BM (1:2 w/w)-based photovoltaic device exhibited PCE of 3.15% with V_{oc} ; 0.75 V, J_{sc} ; 8.59 mA cm⁻², FF; 49% in 2% CB solution. In the case of DIO addition and methanol treatment, PCE of **P2**:PC₇₁BM (1:2 w/w) based device

decreased from 3.15% to 1.89%. The reason of this reduction can be explained with the fewer interconnected domains on treatment.

REFERENCES

- (1) Kiess, H. *Conjugated Conducting Polymers*; Springer-Verlag, 2012; Vol. 102.
- (2) Bokria, J. G. Versatile Route for Syntheses of pi-Conjugated Polymers and Device Fabrication, Ph.D Thesis, University of Connecticut, Connecticut, January 2008.
- (3) McGehee, M. D.; Heeger, A. J. *Adv. Mater.* **2000**, *12* (22), 1655–1668.
- (4) Sirdeshmukh, D. B.; Sirdeshmukh, L.; Subhadra, K. G.; Sunandana, C. S. *Electrical, Electronic and Magnetic Properties of Solids*; 2014; Vol. 207.
- (5) Molapo, K. M.; Ndangili, P. M.; Ajayi, R. F.; Mbambisa, G.; Mailu, S. M.; Njomo, N.; Masikini, M.; Baker, P.; Iwuoha, E. I. *Int. J. Electrochem. Sci.* **2012**, *7* (12), 11859–11875.
- (6) Williams, E. L.; Ang, T. S.; Ooi, Z.; Sonar, P.; Lin, T. T.; Neo, W. T.; Song, J.; Holey, J. *Polymers (Basel)*. **2015**, *7* (1), 69–90.
- (7) Roncali, J. *Macromol. Rapid Commun.* **2007**, *28* (17), 1761–1775.
- (8) Cheng, Y.-J.; Yang, S.-H.; Hsu, C.-S. *Chem. Rev. (Washington, DC, U. S.)* **2009**, *109* (11), 5868–5923.
- (9) Gutzler, R. *Phys. Chem. Chem. Phys.* **2016**, *18* (42), 6537–6554.
- (10) Xu, T.; Yu, L. *Mater. Today* **2014**, *17* (1), 11–15.
- (11) Economy, K.; Tepi, C. *Chem. Chem. Phys.* **2015**, *2* (2), 65–79.
- (12) Brouwer, F. *Developing suitable polymer semiconductors for the application in BioFETs*. Ph.D. Thesis, University of Groningen, Holland, November 2011.
- (13) MacDiarmid, A. G. *Angew. Chemie - Int. Ed.* **2001**, *40* (14), 2581–2590.
- (14) Van Mullekom, H. A. M.; Vekemans, J. A. J. M.; Havinga, E. E.; Meijer, E.

W. Developments in the chemistry and band gap engineering of donor-acceptor substituted conjugated polymers; 2001; Vol. 32.

- (15) Gazotti, W. A.; Nogueira, A. F.; Giroto, E. M.; Micaroni, L.; Martini, M.; das Neves, S.; De Paoli, M.-A. *Chapter 2 – Optical devices based on conductive polymers*; 2001; Vol. 10.
- (16) Lan, L.; Zhang, G.; Dong, Y.; Ying, L.; Huang, F.; Cao, Y. *Polym. (United Kingdom)* **2015**, *67*, 40–46.
- (17) Sharma, B.; Alam, F.; Dutta, V.; Jacob, J. *Org. Electron. physics, Mater. Appl.* **2017**, *40*, 42–50.
- (18) Ding, P.; Zhong, C.; Zou, Y.; Pan, C.; Wu, H.; Cao, Y. *J. Phys. Chem. C* **2011**, *115*, 16211–16219.
- (19) Kim, T.; Chakravarthi, N.; Kumarasamy, G.; Jin, S.-H. *Mol. Cryst. Liq. Cryst.* **2016**, *635* (1), 45–56.
- (20) Zhang, D.; Wang, M.; Liu, X.; Zhao, J. *RSC Adv.* **2016**, *6* (96), 94014–94023.
- (21) Li, J.; Marks, T. J. *Chem. Mater.* **2008**, *20* (15), 4873–4882.
- (22) Wang, M.; Li, C.; Lv, A.; Wang, Z.; Bo, Z.; Zhang, F. *Polymer (Guildf)*. **2012**, *53* (2), 324–332.
- (23) Yu, X.; Yu, J.; Zhou, J.; Huang, J.; Jiang, Y. *Appl. Phys. Lett.* **2011**, *99* (6), 3–6.
- (24) Yen, H.-J.; Liou, G.-S. *Polym. Chem.* **2012**, *3* (2), 255–264.
- (25) Xie, Y.; Peng, Z.; Jia, T.; Zhang, H.; Hou, Q.; Luo, S.; Zeng, R.; Hou, L. *J. Mater. Sci. Mater. Electron.* **2016**, *27* (5), 4705–4710.
- (26) Ning, Z.; Tian, H. *Chem. Commun.* **2009**, *414* (37), 5483.
- (27) Hacıoglu, Serife O., Toksabay, S., Sendur, M., Toppare, L. *Polym. Chem.* **2013**, *52*, 537–544.

- (28) Shi, W.; Zhen, H.; Luo, Y.; Qin, H.; Mi, H.; Awut, T.; Nurulla, I. *Polym. Bull.* **2010**, *64* (1), 53–65.
- (29) Gwinner, M. C.; Brenner, T. J. K.; Lee, J.-K.; Newby, C.; Ober, C. K.; McNeill, C. R.; Siringhaus, H. *J. Mater. Chem.* **2012**, *22* (10), 4436.
- (30) Cheng, H.; Huang, Z.; Wang, L.; Meier, H.; Cao, D. *Dye. Pigment.* **2017**, *137*, 143–151.
- (31) Wallace W. H.; Wong, J. S.; Sreenivasa R.; Puniredd, W.B. *Polym. Chem.* **2014**, *5*, 1258–1263.
- (32) Zhang, Z.; Peng, B.; Liu, B.; Pan, C.; Li, Y.; He, Y.; Zhou, K.; Zou, Y. *Polym. Chem.* **2010**, *1* (9), 1441.
- (33) Erlik, O.; Unlu, N. A.; Hizalan, G.; Hacıoglu, S. O.; Comez, S.; Yildiz, E. D.; Toppare, L.; Cirpan, A. *J. Polym. Sci. Part A Polym. Chem.* **2015**, *53* (13), 1541–1547.
- (34) Wang, X.; Sun, Y.; Chen, S.; Guo, X.; Zhang, M.; Li, X.; Li, Y.; Wang, H. *Macromolecules* **2012**, *45* (3), 1208–1216.
- (35) Luponosov, Y. N.; Solodukhin, a. N.; Ponomarenko, S. a. *Branched triphenylamine-based oligomers for organic electronics*; 2014; Vol. 56.
- (36) Yasuda, T.; Shinohara, Y.; Ishi-I, T.; Han, L. *Org. Electron. physics, Mater. Appl.* **2012**, *13* (10), 1802–1808.
- (37) Zhang, B.; Liang, J.; Hu, L.; Peng, F.; Chen, G.; Yang, W. *J. Mater. Sci.* **2015**, *50* (16), 5609–5619.
- (38) Du, J.; Fortney, A.; Washington, K. E.; Bulumulla, C.; Huang, P.; Dissanayake, D.; Biewer, M. C.; Kowalewski, T.; Stefan, M. C. *ACS Appl. Mater. Interfaces* **2016**, *8* (48), 33025–33033.
- (39) Tao, Q.; Liu, T.; Duan, linrui; Cai, yufeng; Xiong, W.; Wang, P.; Tan, H.; Lei, G.; Pei, Y.; Zhu, W.; Yang, R.; Sun, Y. *J. Mater. Chem. A* **2016**, *4* (48),

18792–18803.

- (40) Raj, M. R.; Kim, M.; Kim, H. Il; Lee, G.-Y.; Park, C. W.; Park, T. *J. Mater. Chem.* **2017**, *5* (7), 3330-3335.
- (41) Zhang, Z.D.; Zhang, K.; Liu, G.; Zhu, C.; Neoh, K.; Kang, E.T. *Macromolecules* **2009**, *42* (8), 3104-3111.
- (42) Banal, J. L.; Subbiah, J.; Graham, H.; Lee, J.-K.; Ghiggino, K. P.; Wong, W. W. H. *Polym. Chem.* **2013**, *4* (4), 1077–1083.
- (43) Kim, J. H.; Kim, H. U.; Lee, J. K.; Park, M. J.; Hyun, M. H.; Hwang, D. H. *Synth. Met.* **2013**, *179*, 18-26.
- (44) Kotowski, D.; Luzzati, S.; Bianchi, G.; Calabrese, A.; Pellegrino, A.; Po, R.; Schimperna, G.; Tacca, A. *J. Mater. Chem. A* **2013**, *1* (36), 10736–10744.
- (45) Goker, S.; Hacıoglu, S. O.; Hizalan, G.; Aktas, E.; Cirpan, A.; Toppare, L. *Macromol. Chem. Phys.* **2017**, *218* (18), 1600544.
- (46) Mortimer, R. J.; Rosseinsky, D. R.; Monk, P. M. S. *Electrochromic Mater. Devices* **2015**, *77*, 1–638.
- (47) Fossatti, D.; José, W.; Maria, R.; Mello, Q. De. *Span* **2011**, *1* (4), 180–191.
- (48) Argun, A. A.; Aubert, P.-H.; Thompson, B. C.; Schwendeman, I.; Gaupp, C. L.; Hwang, J.; Pinto, N. J.; Tanner, D. B.; MacDiarmid, A. G.; Reynolds, J. R. *Chem. Mater.* **2004**, *16* (23), 4401–4412.
- (49) Monk, P. M. S.; Mortimer, R. J.; Rosseinsky, D. R. *Electrochromism : Fundamentals and Applications*; 1995.
- (50) Skotheim, T.A., Reynolds, J. R. *Conjugated Polymers: Theory, Synthesis, Properties and Characterization*, 3rd ed.; New York, 2006; Vol. 1993.
- (51) Beverina, L.; Pagani, G. a; Sassi, M. *Chem. Commun. (Camb)*. **2014**, *50* (41), 5413–5430.

- (52) Mortimer, R. J.; Varley, T. S. *Sol. Energy Mater. Sol. Cells* **2012**, *99*, 213–220.
- (53) Mortimer, R. J. *Electrochim. Acta* **1999**, *44* (18), 2971–2981.
- (54) Argun, A. A. *Patterning of Conjugated Polymers for Electrochromic Devices*. Ph.D Thesis, University of Florida, December 2004.
- (55) Beaujuge, P. M.; Reynolds, J. R. *Chem. Rev.* **2010**, *110* (1), 268–320.
- (56) Monk, Paul M S, Mortimer, R.J, Rosseinsky, D. R. *Electrochromism and Electrochromic Devices*; 2007.
- (57) Kim, T.; Kim, J.-H.; Kang, T. E.; Lee, C.; Kang, H.; Shin, M.; Wang, C.; Ma, B.; Jeong, U.; Kim, T.-S.; Kim, B. J. *Nat. Commun.* **2015**, *6*, 8547.
- (58) Abdulrazzaq, O. a.; Saini, V.; Bourdo, S.; Dervishi, E.; Biris, A. S. *Part. Sci. Technol.* **2013**, *31* (5), 427–442.
- (59) Yu, G.; Gao, J.; Hummelen, J. C.; Wudl, F.; Heeger, A. J. *Science* (80-.). **1995**, *270* (5243), 1789–1791.
- (60) Brabec, C. J.; Cravino, A.; Meissner, D.; Sariciftci, N. S.; Fromherz, T.; Rispiens, M. T.; Sanchez, L.; Hummelen, J. C. *Adv. Funct. Mater.* **2001**, *11* (5), 374–380.
- (61) Tress, W. *Organic Solar Cells*; Springer Series in Materials Science; Springer International Publishing: Cham, 2014; Vol. 208.
- (62) Hansson, R. *Materials and Device Engineering for Efficient and Stable Polymer Solar Cells* *Materials and Device Engineering for Efficient and Stable Polymer Solar Cells*; 2017.
- (63) Vivek, K. a; Agrawal, G. D. *Int. J. Res. Eng. Technol.* **2014**, *3* (9), 2319–2322.
- (64) Khalil, A.; Ahmed, Z.; Touati, F.; Masmoudi, M. *2016 13th Int. Multi-Conference Syst. Signals Devices* **2016**, 342–353.

- (65) Lee, K. H.; Schwenn, P. E.; Smith, A. R. G.; Cavaye, H.; Shaw, P. E.; James, M.; Krueger, K. B.; Gentle, I. R.; Meredith, P.; Burn, P. L. *Adv. Mater.* **2011**, *23* (6), 766–770.
- (66) Gevaerts, V. S. *Morphology control and device optimization for efficient organic solar cells*; 2013.
- (67) Scharber, M. C.; Mühlbacher, D.; Koppe, M.; Denk, P.; Waldauf, C.; Heeger, A. J.; Brabec, C. J. *Adv. Mater.* **2006**, *18* (6), 789–794.
- (68) Elumalai, N. K.; Uddin, A. *Energy Environ. Sci.* **2016**, *9* (2), 391–410.
- (69) Stevens, D. M.; Qin, Y.; Hillmyer, M. a.; Frisbie, C. D. *J. Phys. Chem. C* **2009**, *113* (26), 11408–11415.
- (70) Scharber, M. C.; Sariciftci, N. S. *Prog. Polym. Sci.* **2013**, *38* (12), 1929–1940.
- (71) Lu, N.; Li, L.; Sun, P.; Liu, M. *Chem. Phys. Lett.* **2014**, *614*, 27–30.
- (72) Temiz, C. *Benzotriazole and Quinoxaline Containing Random Copolymers for Bulk-Heterojunction Polymer Solar Cell Applications*. M.S. Thesis, Middle East Technical University, Turkey, September, **2015**.
- (73) Erlik, O. *Synthesis and Optoelectronic Applications of Benzotriazole and Dibenzosilole Based Alternating Copolymers*, M.S Thesis, Middle East Technical University, Turkey, October, **2014**.
- (74) Lee, J. W.; Ahn, H.; Jo, W. H. *Macromolecules* **2015**, *48* (21), 7836–7842.
- (75) Wang, J.; Kong, L.; Liang, Z. *Macromol. Chem. Phys.* **2016**, *217*, 1513–1520.
- (76) Zhang, Q.; Kelly, M. A.; Hunt, A.; Ade, H.; You, W. *Macromolecules* **2016**, *49* (7), 2533–2540.
- (77) Cevher, S. C.; Unlu, N. A.; Ozelcaglayan, A. C.; Apaydin, D. H.; Udum, Y. A.; Toppare, L.; Cirpan, A. *J. Polym. Sci. Part A Polym. Chem.* **2013**, *51* (9), 1933–1941.

- (78) Chen, S.; Zhang, D.; Wang, M.; Kong, L.; Zhao, J. *New J. Chem.* **2016**, *40* (3), 2178–2188.
- (79) Böckmann, M.; Schemme, T.; Jong, D. H. de; Denz, C.; Heuer, A.; Doltsinis, N. L. *Phys. Chem. Chem. Phys.* **2015**, *17* (43), 28616–28625.
- (80) Yuan, X.; Zhang, W.; Xie, L. H.; Ma, J.; Huang, W.; Liu, W. *J. Phys. Chem. B* **2015**, *119* (32), 10316–10333.
- (81) Baysec, S.; Akbasoglu Unlu, N.; Hacıoglu, S. O.; Arslan Udum, Y.; Cirpan, A.; Toppare, L. *J. Macromol. Sci. Part A* **2014**, *52* (1), 1–9.
- (82) Bin, H.; Xiao, L.; Liu, Y.; Shen, P.; Li, Y. *J. Polym. Sci. Part A Polym. Chem.* **2014**, *52* (14), 1929–1940.
- (83) Zhang, S.; Ye, L.; Wang, Q.; Li, Z.; Guo, X.; Huo, L.; Fan, H.; Hou, J. *J. Phys. Chem. C* **2013**, *117* (19), 9550–9557.
- (84) Goker, S.; Hizalan, G.; Aktas, E.; Kutkan, S.; Cirpan, A.; Toppare, L. *New J. Chem.* **2016**, *40* (12), 10455–10464.
- (85) Wienk, M. M.; Kroon, J. M.; Verhees, W. J. H.; Knol, J.; Hummelen, J. C.; van Hal, P. a; Janssen, R. a J. *Angew. Chem. Int. Ed. Engl.* **2003**, *42* (29), 3371–3375.
- (86) Yang, Y.; Zhang, J.; Zhou, Y.; Zhao, G.; He, C.; Li, Y.; Andersson, M.; Inganäs, O.; Zhang, F. *J. Phys. Chem. C* **2010**, *114* (8), 3701–3706.
- (87) Istanbuluoglu, C.; Gö, S.; Hizalan, G.; Hacıoglu, S. O.; Udum, Y. A.; Yildiz, E. D.; Cirpan, A.; Toppare, L. *New J. Chem. New J. Chem* **2015**, *39* (39), 6623–6630.
- (88) Liu, Y.; Zhao, W.; Wu, Y.; Zhang, J.; Li, G.; Li, W.; Ma, W.; Hou, J.; Bo, Z. *J. Mater. Chem. A* **2016**, *4* (21), 8097–8104.
- (89) Ding, Z.; Kettle, J.; Horie, M.; Chang, S. W.; Smith, G. C.; Shames, A. I.; Katz, E. A. *J. Mater. Chem. A* **2016**, *4* (19), 7274–7280.

- (90) Cetin, A.; Istanbuluoglu, C.; Hacıoglu S. O.; Cevher. S. C.; Udum, Y. A.; Toppare, L.; Cirpan, A. *J. Polym. Sci. Part A Polym. Chem.* **2017**, *55* (27), 3705-3715.

APPENDICES

A. NMR DATA

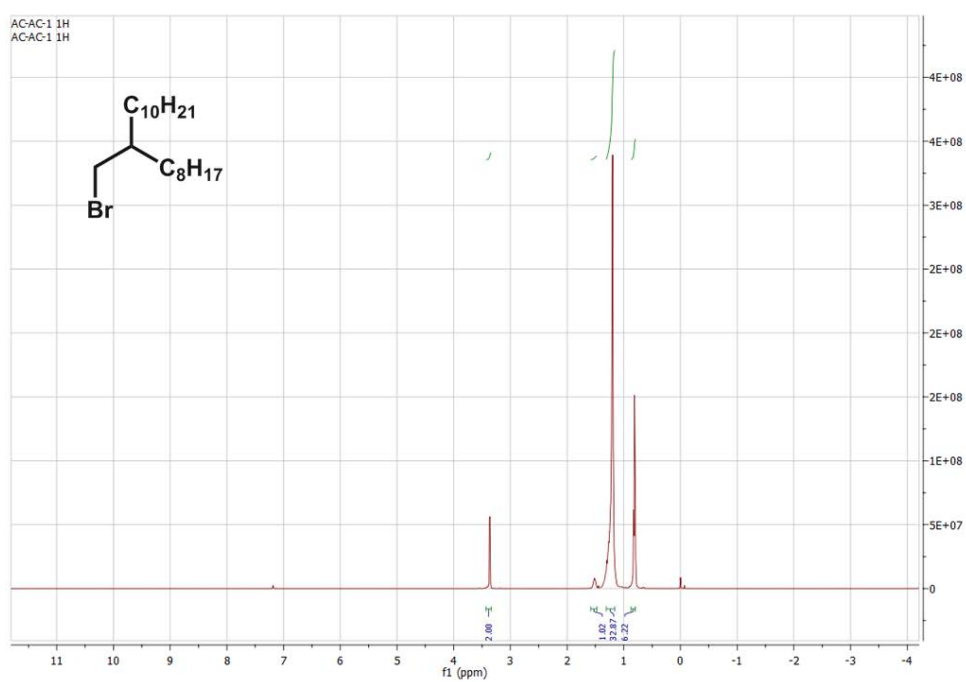


Figure 46. ^1H NMR of 9-(Bromomethyl)nonadecane

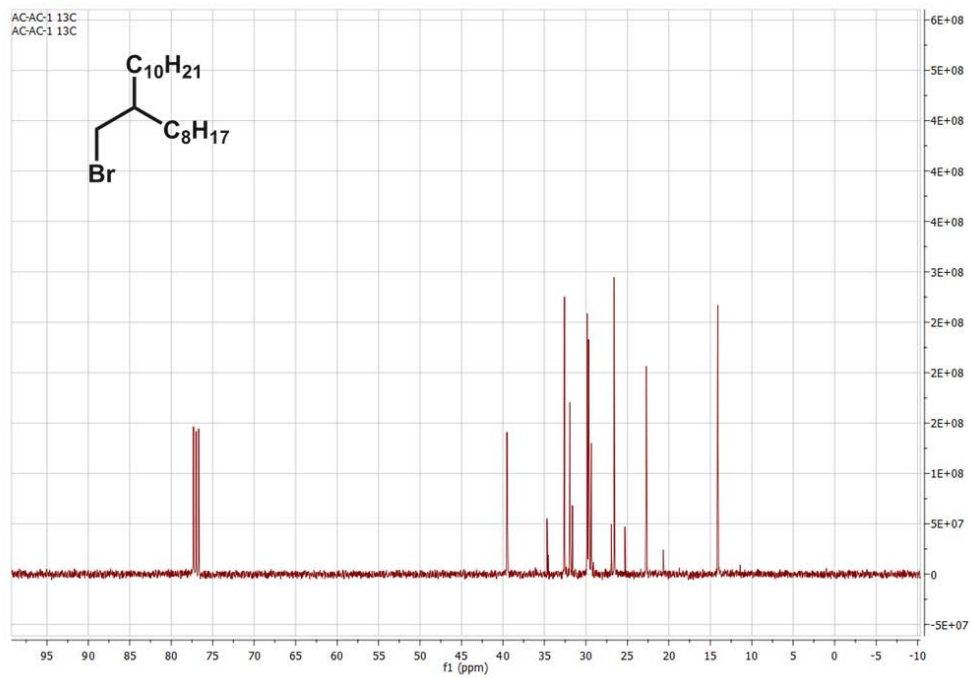


Figure 47. ^{13}C NMR of 9-(Bromomethyl)nonadecane

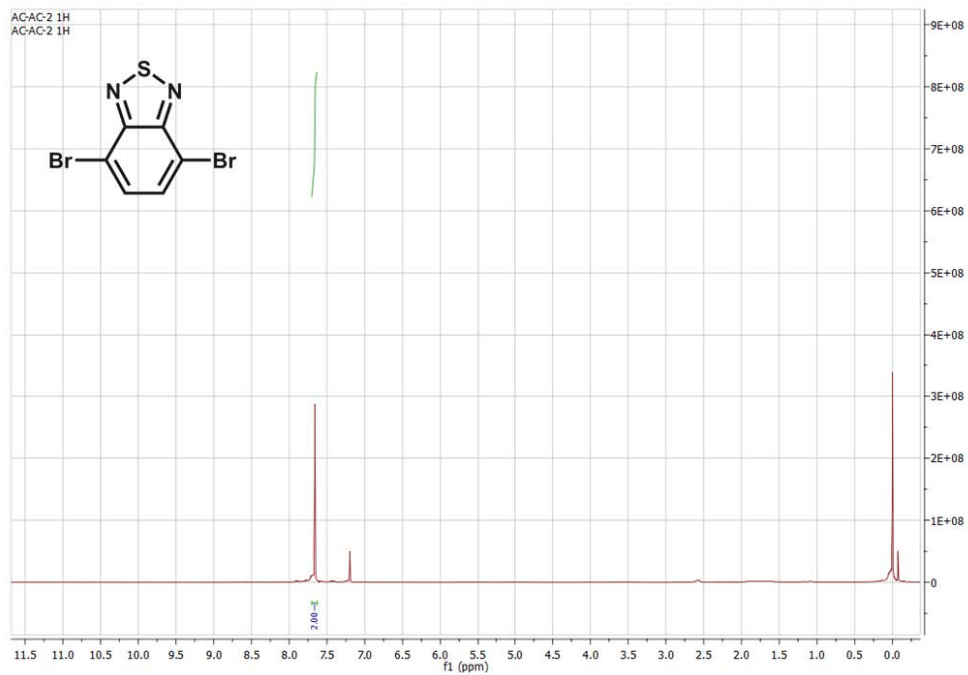


Figure 48. ^1H NMR of 4,7-Dibromobenzo[c][1,2,5]thiadiazole

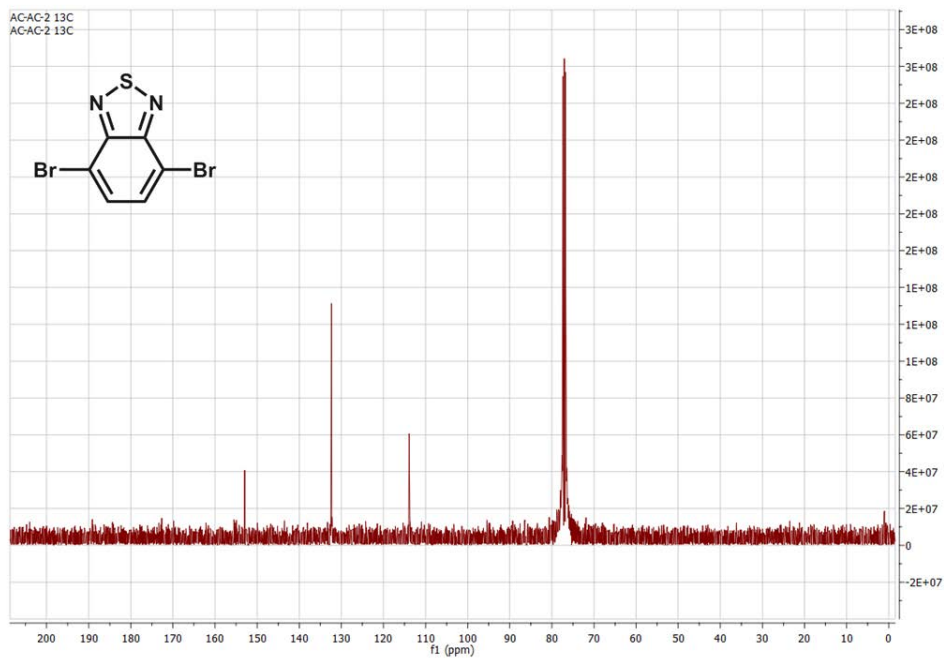


Figure 49. ^{13}C NMR of 4,7-Dibromobenzo[c][1,2,5]thiadiazole

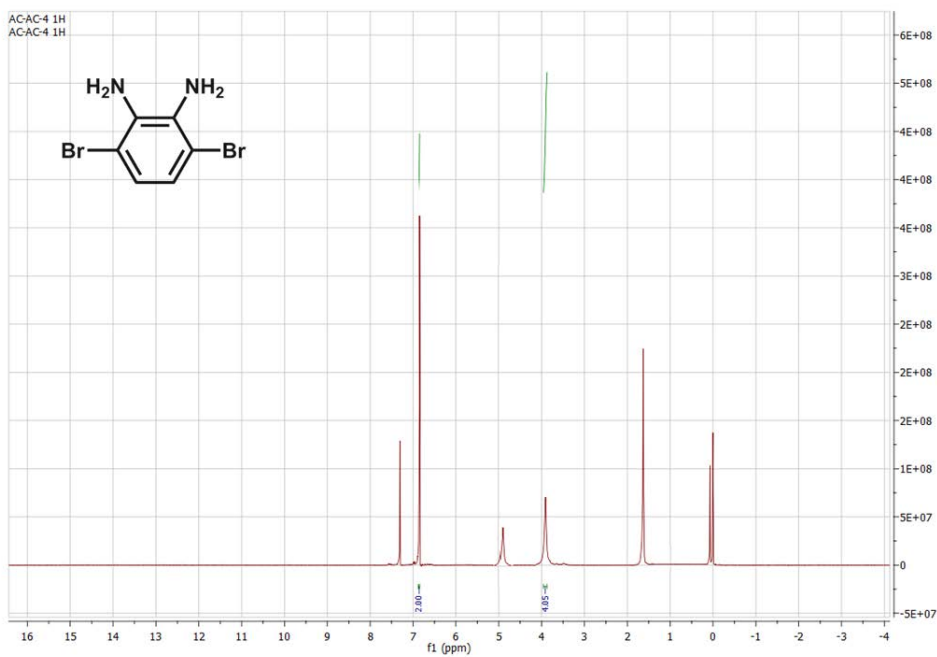


Figure 50. ^1H NMR of 3,6-Dibromobenzene-1,2-diamine

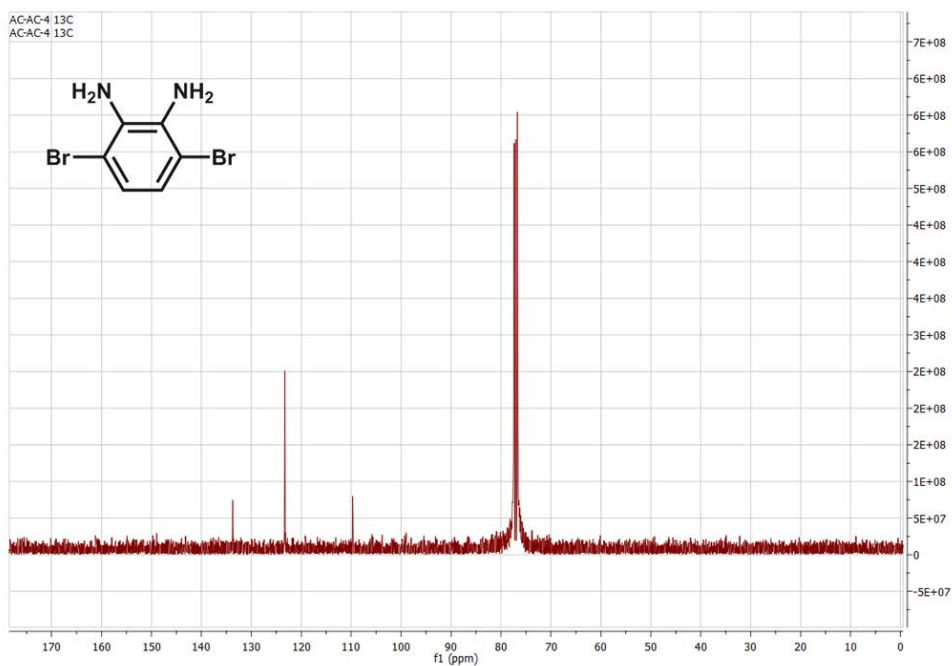


Figure 51. ^{13}C NMR of 3,6-Dibromobenzene-1,2-diamine

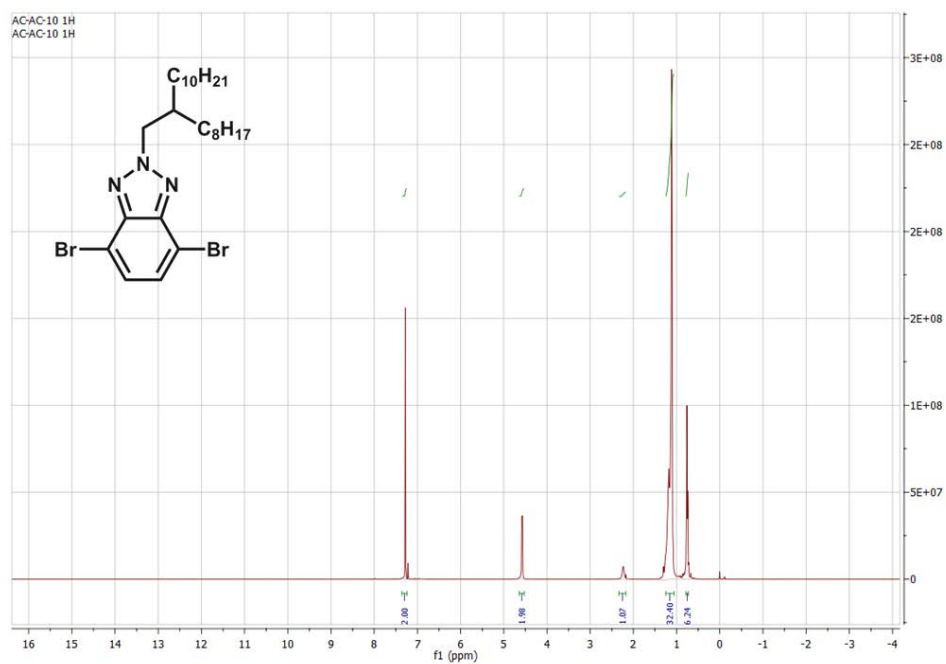


Figure 52. ^1H NMR of 4,7-Dibromo-2-(2-octyldodecyl)-2H-benzo[d][1,2,3]triazole

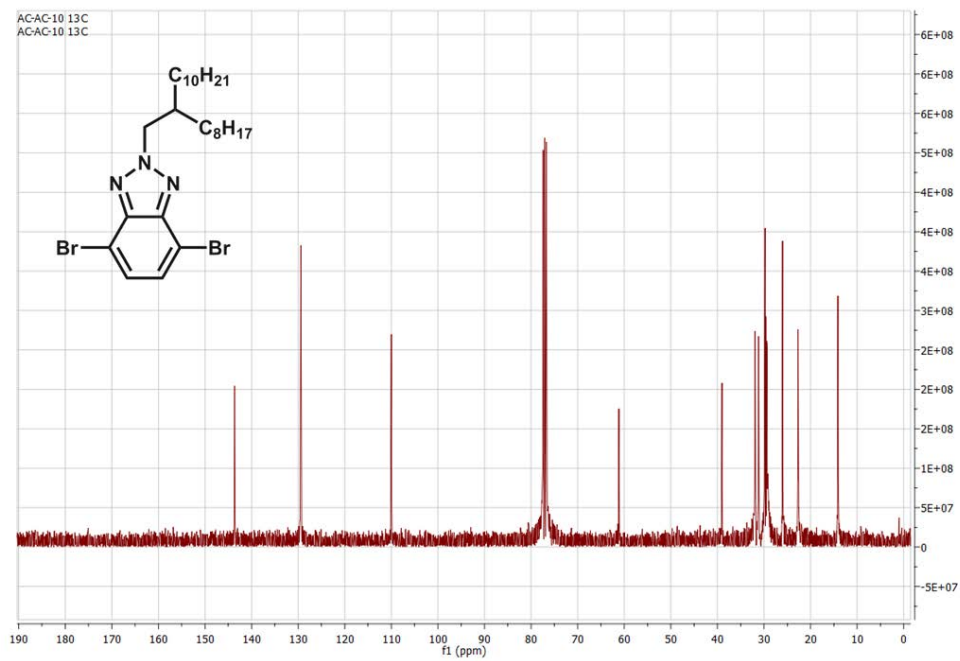


Figure 53. ^{13}C NMR of 4,7-Dibromo-2-(2-octyldodecyl)-2H-benzo[d][1,2,3]triazole

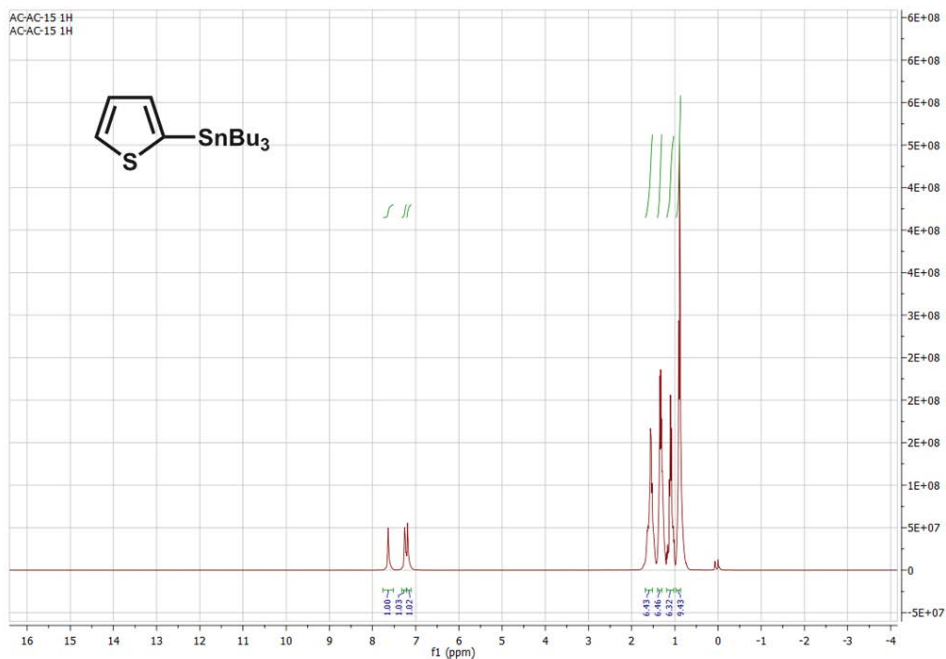


Figure 54. ^1H NMR of Tributyl(thiophene-2-yl)stanne

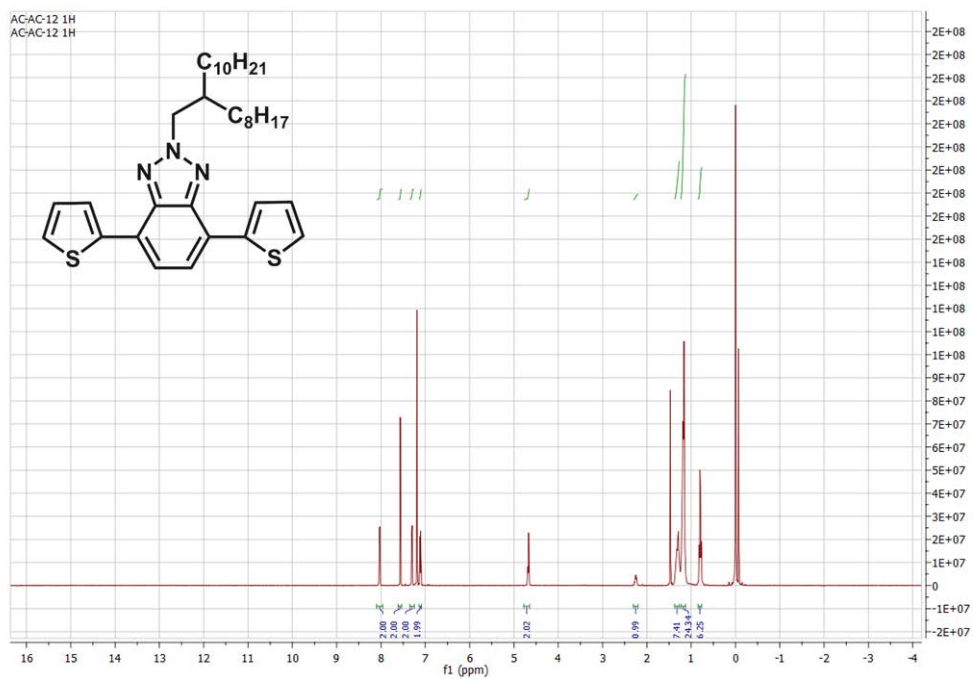


Figure 55. ^1H NMR of 2-(2-Octyldodecyl)-4,7-di(thiophen-2-yl)-2H-benzo[d][1,2,3]triazole

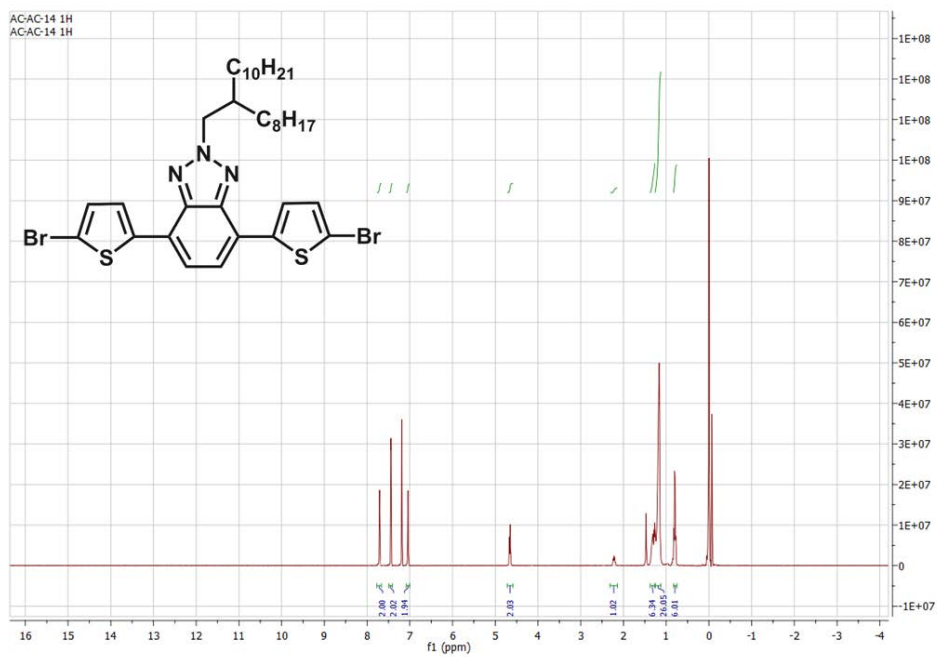


Figure 56. ^1H NMR of 4,7-Bis(5-bromothiophen-2-yl)-2-(2-octyldodecyl)-2H-benzo[d][1,2,3]triazole

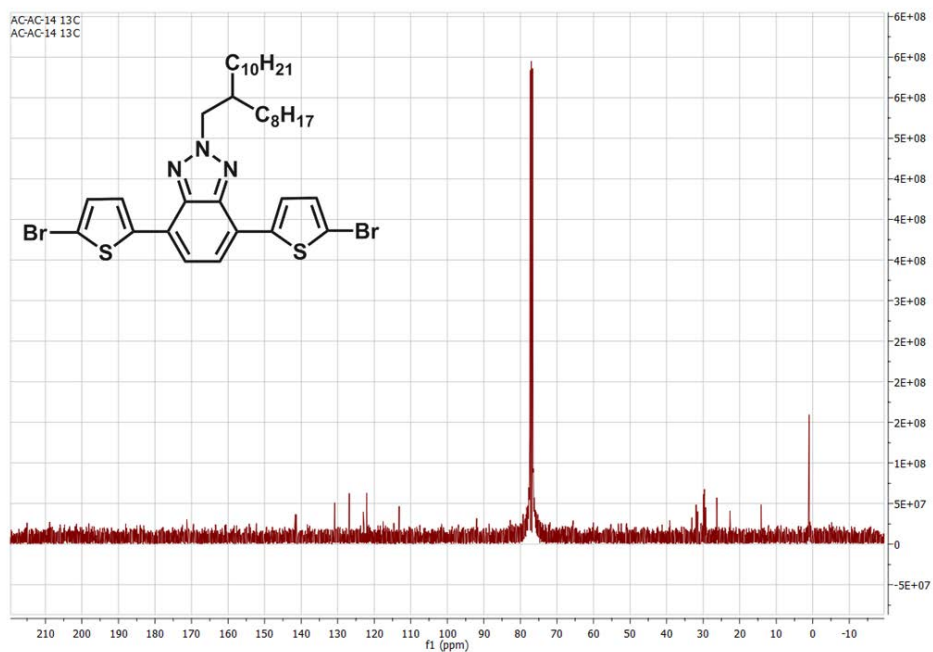


Figure 57. ^{13}C NMR of 4,7-Bis(5-bromothiophen-2-yl)-2-(2-octyldodecyl)-2H-benzo[d][1,2,3]triazole

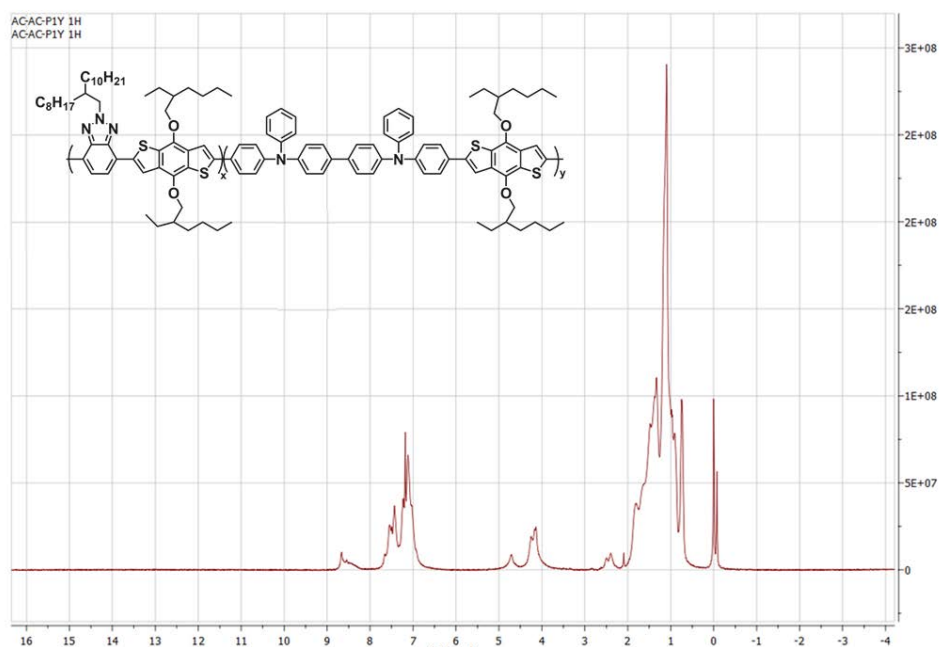


Figure 58. ^1H NMR of P1

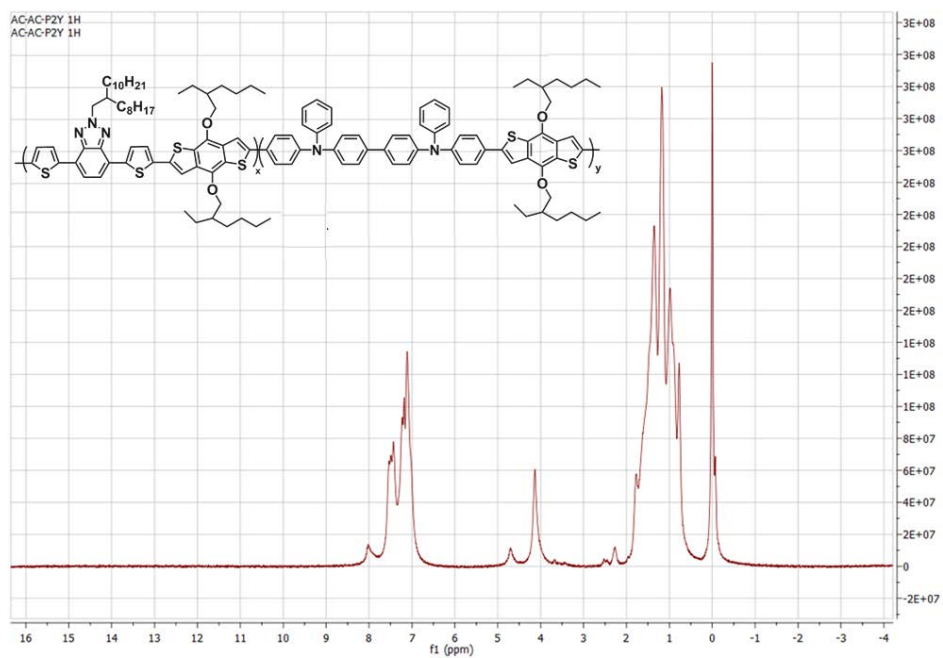


Figure 59. ¹H NMR of P2

B. THERMAL ANALYSIS RESULTS

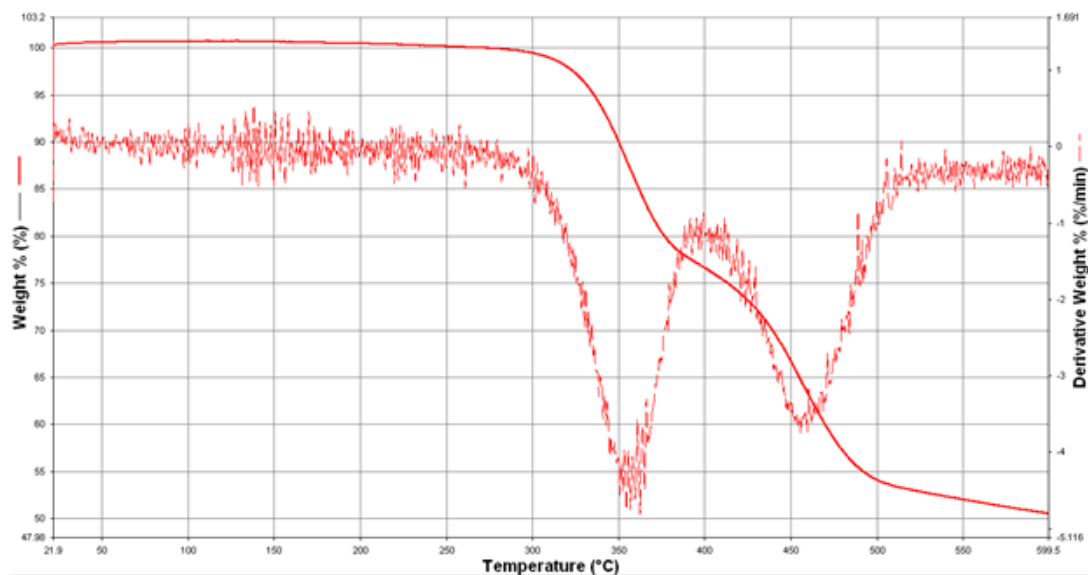


Figure 60. TGA Curve of P1

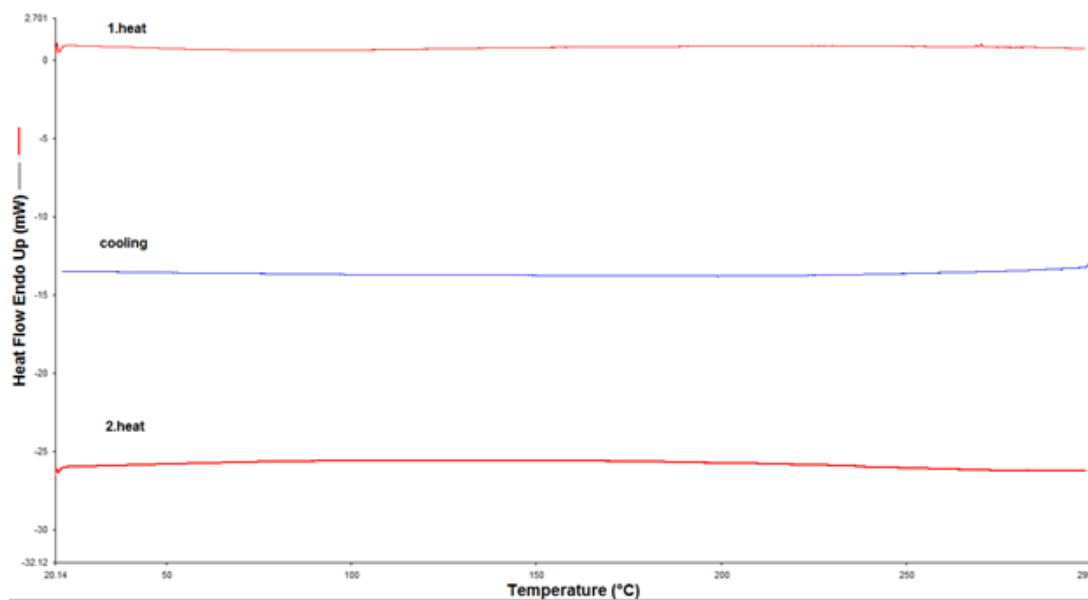


Figure 61. DSC Thermogram of P1

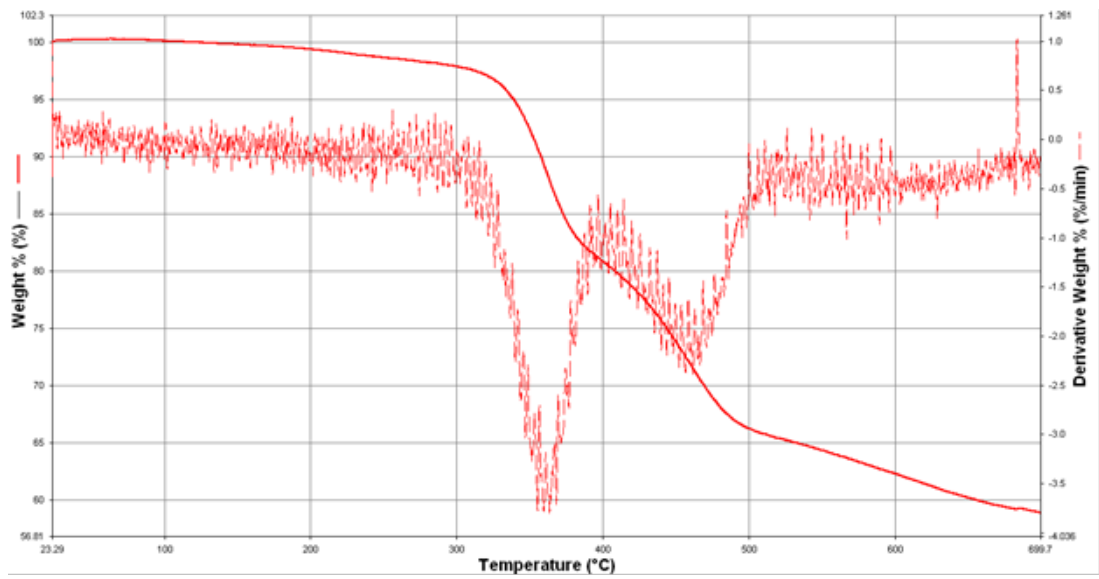


Figure 62. TGA Curve of P2

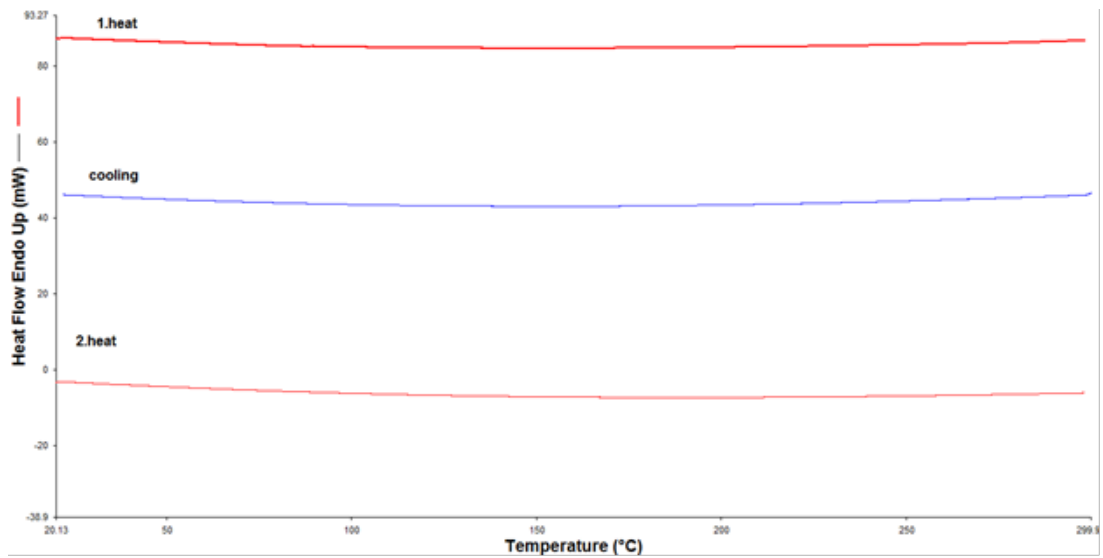


Figure 63. DSC Thermogram of P2